Biogeosciences, 17, 2499–2519, 2020
https://doi.org/10.5194/bg-17-2499-2020

Biogeosciences Open Access EGU

Patterns of (trace) metals and microorganisms in the Rainbow hydrothermal vent plume at the Mid-Atlantic Ridge

Sabine Haalboom[1,★], David M. Price[1,a,★], Furu Mienis[1], Judith D. L. van Bleijswijk[1], Henko C. de Stigter[1], Harry J. Witte[1], Gert-Jan Reichart[1,2], and Gerard C. A. Duineveld[1]

[1]NIOZ Royal Netherlands Institute for Sea Research, department of Ocean Systems, and Utrecht University, P. O. Box 59, 1790 AB Den Burg, Texel, the Netherlands
[2]Utrecht University, Faculty of Geosciences, 3584 CD Utrecht, the Netherlands
[a]current address: University of Southampton, Waterfront Campus, European Way, Southampton, SO14 3ZH, UK
★These authors contributed equally to this work.

Correspondence: Sabine Haalboom (sabine.haalboom@nioz.nl) and David M. Price (d.m.price@soton.ac.uk)

Received: 16 May 2019 – Discussion started: 20 June 2019
Revised: 27 February 2020 – Accepted: 16 March 2020 – Published: 12 May 2020

Abstract. Hydrothermal vent fields found at mid-ocean ridges emit hydrothermal fluids that disperse as neutrally buoyant plumes. From these fluids seafloor massive sulfides (SMS) deposits are formed, which are being explored as possible new mining sites for (trace) metals and rare earth elements (REEs). It has been suggested that during mining activities large amounts of suspended matter will appear in the water column due to excavation processes and discharge of mining waste from the surface vessel. Understanding how hydrothermal plumes can be characterised by means of geochemistry and microbiology as they spread away from their source and how they affect their surrounding environment may help in characterising the behaviour of the dilute distal part of chemically enriched mining plumes.

This study on the extensive Rainbow hydrothermal plume, observed up to 25 km downstream from the vent site, enabled us to investigate how microbial communities and (trace) metal composition change in a natural plume with distance. The (trace) metal and REE content of suspended particulate matter (SPM) was determined using sector field inductively coupled plasma mass spectrometry (SF-ICP-MS) with high resolution (HR), and the microbial communities of the neutrally buoyant plume, above-plume, below-plume, and near-bottom water and sediment were characterised by using 16S rRNA amplicon sequencing methods. Both vertically in the water column and horizontally along the neutrally buoyant plume, geochemical and biological changes were evident, as the neutrally buoyant plume stood out by its enrichments in (trace) metals and REEs, as, for example, Fe, Cu, V, Mn and REEs were enriched by factors of up to ~ 80, ~ 90, ~ 52, ~ 2.5 and ~ 40, respectively, compared to above-plume water samples taken at 1000 m water depth. The concentrations of these elements changed as the plume aged, shown by the decrease in element / Fe molar ratios of chalcophile elements (Cu, Co, Zn), indicative of rapid removal from the hydrothermal plume or removal from the solid phase. Conversely, increasing REE / Fe molar ratios imply uptake of REEs from the ambient seawater onto Fe-oxyhydroxides. This was also reflected in the background pelagic system, as Epsilonproteobacteria started to dominate and univariate microbial biodiversity declined with distance away from the Rainbow hydrothermal vent field. The Rainbow hydrothermal plume provides a geochemically enriched natural environment, which is a heterogeneous, dynamic habitat that is conducive to ecological changes in a short time span. This study of a hydrothermal plume provides a baseline study to characterise the natural plume before the interference of deep-sea mining.

1 Introduction

Hydrothermal vent fields found at mid-ocean ridges and back-arc basins are known for discharging fluids rich in potential microbial energy sources, such as H_2, H_2S, CH_4, NH_4 and Fe (Jannasch and Mottl, 1985; McCollom, 2000). In ad-

dition, they are characterised by the presence of polymetallic sulfide deposits containing high grades of metals like Cu, Co, Zn and rare earth elements (REEs) (Cave et al., 2002; Chavagnac et al., 2005). Because of the steadily increasing demand for these metals and their geopolitical distribution on land, hydrothermal vent deposits are explored as new mining sites (Hoagland, 2010). Since such areas accommodate unique and vulnerable marine life, serious concerns exist about the environmental sustainability of seafloor massive sulfide (SMS) deposit mining (Boschen et al., 2013; Collins et al., 2013), especially with regard to the effects of the different plumes, which are generated during the excavation of ores and by the return flow of wastes in the vicinity of hydrothermal vents (Ramirez-Llodra et al., 2011; Vare et al., 2018). As SMS mining will concentrate on deposits around hydrothermal vents and not on active vents or chimneys due to technical risks associated with high temperatures (Gwyther et al., 2008), it is likely that the background and extinct vent communities (from microorganisms to megafauna) will be impacted through habitat loss, mechanical destruction, noise, smothering and bioaccumulation of toxic substances (Levin et al., 2016). However, knowledge about the background ecosystem and natural plume is sparse, as the vents and their proximal fauna have attracted most of the attention in, for example, microbiology (e.g. Han et al., 2018; Cerqueira et al., 2018).

To fill this gap, the Dutch TREASURE project (STW-NWO) was focussed on describing the structure of the background pelagic and benthic communities of an active hydrothermal vent site with SMS deposits on the Mid-Atlantic Ridge (MAR). The Rainbow hydrothermal vent (36°14′ N on the MAR) was selected for this study as it ejects one of the most prominent and persistent natural plumes on the MAR. Hydrothermal plumes represent a distinct natural ecosystem in itself, which under the influence of currents may extend tens of kilometres away from its point of origin. Basic knowledge of natural plumes is essential to be able to discern impacts arising from future SMS mining plumes created in the vicinity of the hydrothermal vent, which are likely to interfere with the natural hydrothermal plume. Though mining plumes will have a higher initial density and therefore tend to sink rather than maintain buoyancy (Gwyther et al., 2008; Boschen et al., 2013), the finest and slowest-sinking fraction of suspended solids in the mining plume may interfere with the natural plume during its dispersal, especially when released above the seafloor.

Since the discovery of the Rainbow hydrothermal vent field in 1996 by German et al. (1996), several studies concerning the composition of the hydrothermal fluid and the sediment influenced by fallout of particulates from the Rainbow and other hydrothermal plumes have been published. These showed, for example, that the underlying host rock influences the hydrothermal fluid composition (Wetzel and Shock, 2000; Marques et al., 2006). Geochemical investigation of sediment by Cave et al. (2002) at distances of 2 to 25 km from the Rainbow hydrothermal vent field showed enrichments of Fe, Cu, Mn, V, As and P, as well as REEs (Chavagnac et al., 2005), as a result of fallout from the hydrothermal plume. It has further been shown that microbial activity influences geochemical processes in the plume (Breier et al., 2012; Dick et al., 2013), such as scavenging and oxidation of metals (Cowen and Bruland, 1985; Cowen et al., 1990; Mandernack and Tebo, 1993; Dick et al., 2009), influencing the local ocean geochemistry.

Microbial activity within the plume is fuelled by redox reactions that provide energy for chemolithoautotrophic microbial taxa. The abundance of energy sources within plumes and hydrothermal systems support a plethora of chemolithoautotrophic microbial communities (e.g. Orcutt et al., 2011; Frank et al., 2013; Anantharaman et al., 2016). Plume microbial communities can be distinct or relatively similar to background communities (Dick and Tebo et al., 2010; Sheik et al., 2015; Olins et al., 2017), with plume-associated bacteria originating from either seafloor communities, background seawater communities or from growth within the plume (Dick et al., 2013). Djurhuus et al. (2017) observed the reduction in dominance of vent-associated microorganisms with increased redox potential, suggesting that communities associated with the initial rising plume become diluted on a scale of metres. Comparatively little is known about changes in chemical composition and microbial assemblages in the hydrothermal plume after its initial rise, when it becomes neutrally buoyant and is dispersed by currents, remaining traceable in particulate form at least 50 km away from its source (Severmann et al., 2004) and even up to 4000 km in dissolved form (Resing et al., 2015). Considering the majority of microbial growth is predicted to occur in the neutrally buoyant portion of the plume (Reed et al., 2015), further efforts should be concentrated on sampling this portion of the plume.

In order to address this gap, water column and sediment samples from the Rainbow hydrothermal vent area were investigated during the TREASURE cruise. Geochemical and biological changes were explored vertically in the water column and horizontally along the neutrally buoyant plume using sector field inductively coupled plasma mass spectrometry (SF-ICP-MS) with high resolution (HR) to determine the (trace) metal and REE content of the suspended particulate matter (SPM). Next-generation sequencing methods were used to quantify the microbial diversity in the pelagic system, which was influenced by the hydrothermal plume. Whilst mechanical understanding of microbial and geochemical interactions in the plume would have required a different experimental setup, which was beyond the scope of the TREASURE project, this paper aims to contribute to knowledge of geochemical and biological heterogeneity in the surroundings of an SMS site, induced by the presence of an active hydrothermal plume, which should be taken into account in environmental impact assessments of SMS mining.

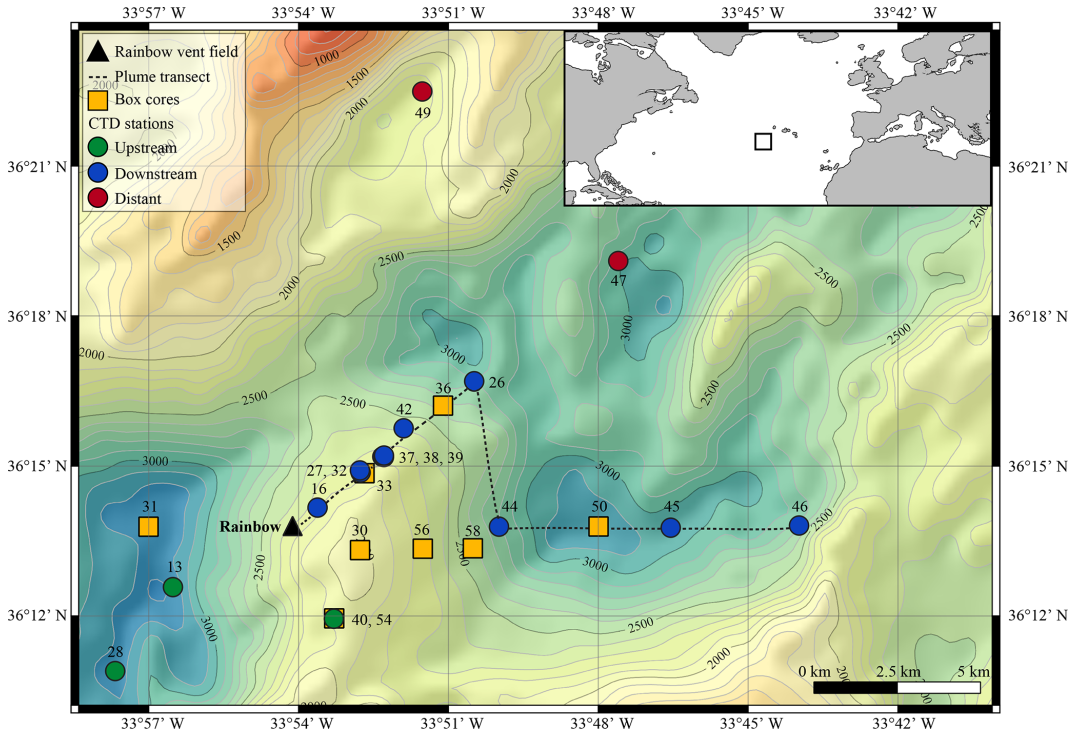

Figure 1. Geographical location (inset) and bathymetric map of the Rainbow study site on the Mid-Atlantic Ridge (from the European Marine Observations and Data Network, EMOD, database), with sampling locations depicted.

2 Material and methods

2.1 Study site

The Rainbow hydrothermal vent field (Fig. 1) is located on the Mid-Atlantic Ridge (MAR) at 36°13.80 N, 33°54.14 W, at approximately 2300 m water depth, southwest of the Azores. The vent field is located on the western flank on the non-volcanic Rainbow Ridge, in an offset between the South Alvin Mid-Atlantic Ridge (AMAR) and AMAR segments of the MAR (German et al., 1996; Fouquet et al., 1998; Douville et al., 2002). It is located at the intersection between the non-transform fault system and the ridge faults (Charlou et al., 2002), making this vent field tectonically controlled. The vent field, which is approximately 100 m by 250 m in size, is underlain by a basement composed of ultramafic rocks (Edmonds and German, 2004; Marques et al., 2006). The ultramafic setting of Rainbow is atypical for the region, which is dominated by basalt-hosted vent systems (Douville et al., 2002). Due to serpentinisation reactions during the circulation of the hydrothermal fluid in the peridotite basement rocks, the Rainbow vent field produced plumes particularly enriched in transition metals (notably Fe, Mn and Cu) and REEs (Douville et al., 2002; Findlay et al., 2015). On the contrary, the plumes are depleted in hydrogen sulfides (Charlou et al., 2002; Douville et al., 2002), resulting in relatively high metal / sulfide ratios. Consequently, the chimneys and the SMS deposits of the Rainbow hydrothermal field are enriched in Cu, Zn, Co and Ni when compared to vent systems with a basaltic host rock (Charlou et al., 2002).

The vent field consists of 10 active, high-temperature (365 °C), black smokers and emits an extensive plume with a distinct chemical composition compared to the ambient seawater (Severmann et al., 2004). The plume is considered the largest and widest spreading in the region (German et al., 1996), rising up to 200 m above its source and traceable over at least 50 km (Severmann et al., 2004). Controlled by the local hydrodynamic regime and topography (Thurnherr and Richards, 2001; Thurnherr et al., 2002), the neutrally buoyant plume moves predominantly to the north and east around the Rainbow Ridge with an average current speed of 5–6 cm s^{-1} and continues in a northward direction along the southern and eastern side of the rift valley of the AMAR segments (Edmonds and German, 2004). Characteristics and behaviour of the Rainbow plume are relatively well studied, which make the Rainbow vent field a suitable site to study neutrally buoyant plumes.

2.2 Water column and sediment sampling

Water samples and sediment cores were collected along the path of the plume during RV *Pelagia* cruise 64PE398 in April 2015. Five putatively distinct biotopes were sampled: (i) above-plume (1000 m water depth), (ii) plume, (iii) below-plume (10 m above the bottom), (iv) near-bottom water and (v) sediment.

Using conductivity, temperature and depth (CTD) casts with a Seabird 911 CTD rosette system, the plume was traced in real time using turbidity as an indicator, measured in Nepheloid Turbidity Units (NTUs) with a WetLabs turbidity sensor. Other variables measured included temperature (°C), salinity, density ($\sigma - \theta, \mathrm{kg\,m^{-3}}$), dissolved oxygen ($\mathrm{ml\,L^{-1}}$) and chlorophyll ($\mu\mathrm{g\,L^{-1}}$). At five stations, continuous yo-yo CTD casts were taken over the course of 12 h to study the temporal changes of the hydrothermal plume.

A total of 41 water samples were collected using 12 L Niskin bottles from 11 downstream stations, 2 distal downstream stations and 3 upstream stations. Once the CTD was back on deck, three distinct water samples were immediately taken for SPM, trace metals and the microbial community.

Depths for sampling SPM were chosen to comprise the largest variation in turbidity measured by the WetLabs turbidity sensor in a vertical profile so that the sensor could be reliably calibrated and readings converted to milligrams per litre. If possible, trace metal and microbial community samples were taken at the same stations and/or same depth.

Sediment and near-bottom water samples were collected with a NIOZ-designed box corer of 50 cm diameter equipped with a top valve to prevent flushing, subsequently trapping near-bottom water (van Bleijswijk et al., 2015). In total, eight cores were collected (Table 1). Due to unsuitable coring substrates, CTD locations and coring sites did not always follow the same track. Box cores were taken on the eastern part of the Rainbow Ridge, continuing in the basin east of the ridge, while two cores were taken on the northwestern flank of the ridge, following the path of the plume.

2.3 Suspended particulate matter analysis

From each 12 L Niskin bottle, two 5 L subsamples were collected to determine the concentration of SPM. The subsamples were filtered on board over pre-weighed 0.4 µm polycarbonate filters. The filters were rinsed with $\sim$ 10 mL of Milli-Q water to remove salt while still applying under pressure and subsequently stored at −20 °C on board. In the laboratory, the filters were freeze dried and then weighed in duplicate, or in triplicate if the difference between the first two measurements was more than 0.03 mg. To yield SPM concentrations, the net dry weight of the SPM collected on the filters (average of 0.25 mg), corrected by the average weight change of all blank filters (0.04 mg), was divided by the volume of filtered seawater (5 L). Subsequently, the filters were examined using a Hitachi TM3000 tabletop scanning electron microscope (SEM) connected to an energy-dispersive spectroscopy (EDS) detector to visualise content of the SPM and to qualitatively analyse the chemical composition. The SEM was operated under an acceleration voltage of 15 kV and a filament current of 1850 mA.

2.4 Chemical analysis

For analysis of major and trace metals present in particulate form in and around the hydrothermal plume, water samples were filtered on board over acid-cleaned 0.45 µm polysulfone filters directly from the Niskin bottle at ambient temperature while applying under pressure. A water barrel in between the filtration holder and pump allowed for volume measurements of filtered water. The filters were subsequently stored at −20 °C until further examination. Filters were dried in the laboratory in an Interflow laminar flow bench at room temperature prior to analysis. Subsequently, the filters were placed in acid-cleaned Teflon vials and were subjected to a total digestion method. For this purpose a mixture of 6.5 mL HNO_3 (ultrapure) / HF (suprapure) (10 : 1) solution, 1 mL HCl (ultrapure) and 1 mL $HClO_4$ (ultrapure) was added to the vials, after which the vials were covered and placed in an Analab HotBlock for 48 h at 125 °C. After the filters were completely dissolved, the covers were taken off from the vials and the vials were left for 24 h in order to evaporate the acids. Finally, the residue was taken up again in 10 mL 1M ultra grade HNO_3, and pre-spiked with 5 ppb scandium and 5 ppb rhodium as internal standards. Furthermore, 10 procedural blanks were performed. Half of them were empty acid-cleaned Teflon vials, the other five contained an acid-cleaned blank filter in order to correct for the dissolved filters. These blanks were subjected to the same total digestion method as described above. A SF-ICP-MS (Thermo Element II) at the Royal Netherlands Institute for Sea Research (NIOZ) was used to analyse the concentrations of major and trace metals, as well as REEs. The concentrations were calculated using external calibration lines made from a multi-stock solution, which was prepared by mixing Fluka TraceCert standards for ICP. Rh was used as an internal standard for all elements. The machine drift was measured before, halfway and after each series of samples and was monitored by using an external drift solution. Precision (relative standard deviation, RSD) of these analyses was generally $< 2\,\%$ for major and trace metals, apart from ^{115}In, where the RSD values generally are between 4 % and 8 %, with maximum values going up to 12.48 %. For REEs, the RSD values were generally $< 3\,\%$, apart from a few measurements where RSD values reached maximums up to 12.48 %. The accuracy could not be determined as no certified reference material was analysed. A blank correction was applied to the sample data by subtracting average values measured for five dissolved blank filters, which for the majority of the measured elements accounted for less than 10 % of the sample values. Subsequently, the data were recalculated to account for the dilution of the samples during the total digestion and the amount of seawater that was filtered to yield the true concentration of each element.

Table 1. Metadata of samples taken.

Station	Latitude	Longitude	Biotope	Sample type	Depth (m)	Micro-biology	SPM	(Trace) metals
30	36°13′19″N	33°52′46″W	Sediment and near-bottom water	Box core	1970	x		
31	36°13′47″N	33°57′00″W	Sediment and near-bottom water	Box core	3190	x		
33	36°14′51″N	33°52′41″W	Sediment and near-bottom water	Box core	2223	x		
36	36°16′13″N	33°51′06″W	Sediment and near-bottom water	Box core	2857	x		
50	36°13′47″N	33°47′60″W	Sediment and near-bottom water	Box core	3157	x		
54	36°11′57″N	33°53′46″W	Sediment and near-bottom water	Box core	2129	x		
56	36°13′21″N	33°51′31″W	Sediment and near-bottom water	Box core	2198	x		
58	36°13′21″N	33°50′31″W	Sediment and near-bottom water	Box core	2514	x		
13	36°12′35″N	33°56′31″W	Above-plume	CTD	125	x		
13	36°12′35″N	33°56′31″W	Below-plume	CTD	3220	x		
13	36°12′35″N	33°56′31″W	Plume	CTD	2000	x		
16	36°14′10″N	33°53′37″W	Plume	CTD	1944	x		
16	36°14′10″N	33°53′37″W	Above-plume	CTD	998	x		
26	36°16′41″N	33°50′29″W	Below-plume	CTD	2756	x	x	x
26	36°16′41″N	33°50′29″W	Plume	CTD	2150	x	x	x
26	36°16′41″N	33°50′29″W	Plume	CTD	2000		x	x
26	36°16′41″N	33°50′29″W	Above-plume	CTD	999	x	x	x
27	36°16′52″N	33°52′45″W	Below-plume	CTD	2191	x		x
27	36°16′52″N	33°52′45″W	Plume	CTD	2077	x		x
27	36°16′52″N	33°52′45″W	Plume	CTD	1996			x
27	36°16′52″N	33°52′45″W	Above-plume	CTD	994	x		x
28	36°10′54″N	33°57′40″W	Below-plume	CTD	3170	x	x	x
28	36°10′54″N	33°57′40″W	Plume	CTD	1975	x	x	x
32	36°14′55″N	33°52′46″W	Plume	CTD	2192		x	
32	36°14′55″N	33°52′46″W	Plume	CTD	2088		x	
37	36°15′11″N	33°52′19″W	Plume	CTD	2190			x
38	36°15′11″N	33°52′17″W	Plume	CTD	2040			x
39	36°15′13″N	33°52′17″W	Plume	CTD	2019			x
40	36°11′57″N	33°53′18″W	No plume	CTD	2120			x
42	36°15′45″N	33°51′54″W	Plume	CTD	2291	x	x	x
42	36°15′45″N	33°51′54″W	Plume	CTD	2209	x	x	x
42	36°15′45″N	33°51′54″W	Plume	CTD	2037		x	x
42	36°15′45″N	33°51′54″W	Above-plume	CTD	999	x	x	x
44	36°13′47″N	33°49′59″W	Below-plume	CTD	2623	x		
44	36°13′47″N	33°49′59″W	Plume	CTD	2202		x	x
44	36°13′47″N	33°49′59″W	Plume	CTD	2002	x	x	x
44	36°13′47″N	33°49′59″W	Above-plume	CTD	995	x		
45	36°13′46″N	33°46′33″W	Below-plume	CTD	3004	x		
45	36°13′46″N	33°46′33″W	Plume	CTD	2166		x	x
45	36°13′46″N	33°46′33″W	Plume	CTD	2002	x	x	x
45	36°13′46″N	33°46′33″W	Above-plume	CTD	996	x		
46	36°13′49″N	33°43′59″W	Below-plume	CTD	2622	x		
46	36°13′49″N	33°43′59″W	Plume	CTD	2280	x	x	x
46	36°13′49″N	33°43′59″W	Plume	CTD	2145		x	x
46	36°13′49″N	33°43′59″W	Above-plume	CTD	1000	x		
47	36°19′06″N	33°47′36″W	Below-plume	CTD	2850			
47	36°19′06″N	33°47′36″W	Plume	CTD	2200	x		x
49	36°22′19″N	33°51′31″W	Plume	CTD	2260	x	x	x
49	36°22′19″N	33°51′31″W	Plume	CTD	1902		x	x

2.5 Microbial community

Three distinct samples of 2 L of water were collected from three different Niskin bottles for next-generation sequencing (NGS). The water was filtered immediately after collection through a 0.2 µm polycarbonate filter (Nuclepore), facilitated by a vacuum of 0.2 bar, in a climate-controlled room at 4 °C to limit DNA degradation. From the box cores > 0.25 g of surface sediment was scraped off with a sterilised spatula, whilst 1.5 L of overlying (near-bottom) water was filtered as above. Filters were stored in a 2 mL cryo-vial and all samples were stored at −80 °C on board.

DNA was extracted using a Power Soil DNA Isolation Kit (MoBio, now Qiagen) according to the manufacturer's protocol. Each DNA extract concentration was quantified using a Qubit 3.0 fluorimeter (Qiagen, Inc.) and stored at −20 °C before amplification. Extracts were combined with Phusion Taq (Thermo Scientific), High-Fidelity Phusion polymerase buffer and universal primers to amplify the V4 region of 16S rDNA of bacteria and archaea (Table 2), with unique molecular identifier (MID) combinations to identify the different samples. All negative controls from all polymerase chain reaction (PCR) series were labelled with the same unique MID. The PCR settings were as follows: 30 s at 98 °C, 29 cycles (10 s at 98 °C, 20 s at 53 °C, 30 s at 72 °C) and 7 min at 72 °C. Four and three samples were rerun at 30 and 32 cycles, respectively, in order to yield enough product. Each sample was subjected to the PCR protocol in triplicate and processed independently to avoid bias. A total of 5 µL of product was used to screen the products on an agarose gel. The remaining 25 µL of each triplicate was pooled to evenly distribute the DNA, split into two slots and run on a 2 % agarose gel at 75 volts for 50 min. Sybergold stain was applied post-run for 20–30 min before cutting the 380 bp bands out with a sterilised scalpel over a blue light to avoid UV damage. The two bands of mixed triplicates were pooled, purified using the Qiaquick Gel Extraction Kit (Qiagen, Inc.) and quantified with a Qubit™ 3.0 fluorometer (Qiagen, Inc.). Samples were pooled in equimolar quantities together with blank PCR controls. The pooled sample was concentrated using MinElute™ PCR Purification columns (Qiagen Inc.) as described by the manufacturer and sent to Macrogen (South Korea) for sequencing. Sequencing was undertaken with a Roches GS FLX instrument using Titanium chemistry on an eight-region gasket and Roche GS FLX instruments. Sequence processing was undertaken as described by van Bleijswijk et al. (2015), using a QIIME pipeline. Sequences shorter than 250 bases and average Q scores below 25 were removed. The OTU sequences (> 98 % similarity) were classified (> 93 % similarity) based on a recent SILVA SSU database (release 132; Yilmaz et al., 2014). Single reads were excluded and all data were standardised to remove any disproportionate sampling bias.

2.6 Statistics

Unconstrained ordination techniques were utilised to distinguish biotopes and general community patterns. Non-metric multidimensional scaling plots (NMDS) were created based upon Bray–Curtis similarity matrices of square-root-transformed microbial community assemblages. Group average clustering was also utilised in order to quantify similarities between the samples. ANalysis Of SIMilarities (ANOSIM) was subsequently used to statistically test community distinctions based upon presumed biotopes (sediment, near-bottom water, below-plume water, plume water and above-plume water). In addition, all water column samples were plotted in separate NMDS plots to observe patterns in greater detail. Physical properties of all water samples (station, depth, turbidity and location) were depicted in a NMDS plot to observe sample similarities. These environmental data were normalised, and Euclidean distance was used to create a similarity matrix. The relationship between Fe and turbidity was tested with a linear regression analysis. Trace metals and REEs were normalised to Fe, since it is the primary particle-forming element at all stages of plume dispersion, giving insight into the chemical behaviour. All multivariate statistics were undertaken in Primer™ V6 (Clarke and Gorley, 2006).

The Shannon–Wiener index ($\log_e$) was calculated as a diversity measure. Biodiversity differences between biotopes were tested with the non-parametric Kruskal–Wallis test with pairwise comparisons, as the data did not meet normality or homogeneity assumptions, even after transformation. These statistical tests were undertaken in SPSS.

A SIMililarities PERcentage analysis (SIMPER in Primer v6) was applied on the microbial class level with a cut-off for low contributions at 90 % based on Bray–Curtis similarity matrix to characterise the community composition based on groups contributing to intra-biotope similarities. Relationships between environmental variables and microbial classes as a percentage of each composition within the plume were tested with Pearson correlation and hierarchical clustering to identify broad response groups.

3 Results

3.1 Water column characteristics

Temperature, salinity and density plots indicated that the water column at each location had similar physical traits, whereby three main different water masses could be distinguished (Fig. S1 in the Supplement). The surface Eastern North Atlantic Central Water (ENACW) was characterised by a temperature, salinity and density at the surface of 18 °C, 36.4 and 26.2 kg m^{-3} to 11 °C, 35.5 and 27.2 kg m^{-3} at the bottom of the water mass. The underlying Mediterranean Outflow Water (MOW) was characterised by a temperature of 7.5–11 °C, a salinity of 35.4–35.5 and a den-

Table 2. Primers used for sequencing.

Forward primer name	Forward primer sequence 5′-3′	Reverse primer name	Reverse primer sequence 5′-3′	Ratio in mix	Reference
Arch-0519-a-S-1 (universal)	CAGCMGCCGCGGTAA	Bact-0785-b-A-18 (universal)	TACNVGGGTATCTAATCC	3/9 + 3/9	Klindworth et al. (2013)
Bact-0519F (targets WS6, TM7, OP11 groups)	CAGCAGCATCGGTVA			1/9	This paper
Nano-0519F (targets Nanoarchaea)	CAGTCGCCRCGGGAA	Nano-0785R (targets Nanoarchaea)	TACNVGGGTMTCTAATYY	1/9 + 1/9	This paper

sity of 27.2–27.75 kg m^{-3}. The North Atlantic Deep Water (NADW) was characterised by temperatures ranging from 4 to 7.5 °C, salinity of 35.0 to 35.4 and a density of 27.75 to 27.825 kg m^{-3} (Emery and Meincke, 1986). The neutrally buoyant plume was centred around the 27.82 kg m^{-3} isopycnal, as illustrated in Figs. 2 and 3.

3.2 Turbidity and plume dispersion

Against a background of non-plume-influenced waters, as found in the CTD casts, with typical concentrations of SPM of 0.04 mg L^{-1} (0.015 NTU), the neutrally buoyant plume stands out as a layer with distinctly higher turbidity values (i.e. higher SPM concentrations) consistently present in the depth interval of 1750–2400 m at stations located north and east of Rainbow (Fig. 2). Except where this turbid water layer was found impinging the seabed, relatively clear waters separated the turbid layer from the underlying seabed.

At downstream stations, a consistent trend of decreasing turbidity and increasing vertical dispersion was noted. At station 27, 3.5 km north of Rainbow, maximum turbidity in the core of the plume was 0.15 NTU (0.09 mg L^{-1}) and plume thickness was about 105 m, whilst at station 46, 15.2 km east of Rainbow, maximum turbidity was only 0.08 NTU (0.06 mg L^{-1}) and plume thickness was 275 m. Away from the main plume path, stations 47 and 49 (13.8 and 16.5 km from Rainbow, respectively) showed a diluted signature similar to that observed at the most distal stations along the main plume path. Despite being most proximal to Rainbow, station 16, located 1.0 km downstream of Rainbow, showed a relatively low turbidity of 0.015 NTU (0.04 mg L^{-1}). Since the plume is more constrained closer to the source, the main body of the narrower plume could have been missed with the CTD. Stations upstream of the vent site (stations 13 and 28, 4.2 and 7.5 km southwest of Rainbow, respectively, and station 40, 3.6 southeast of Rainbow) displayed low turbidity values, ranging between 0.01 and 0.02 NTU (0.04 mg L^{-1}) (Fig. S2).

The CTD profiles from stations 42 and 49 (4.9 and 16.5 km north of Rainbow, respectively) both displayed the highest turbidity in the lower hundreds of metres above the seafloor, with instances of seafloor contact during time of sampling. Therefore, no samples could be taken below the plume at these stations. The assumption that the plume is subject to vertical movement is supported by observations made during 12 h CTD yo-yo casts carried out at station 27 (Fig. 3). Along with vertical displacements of the 27.82 kg m^{-3} isopycnal on the order of 150 m, likely reflecting internal tidal motions, the hydrothermal plume was found to also move up and down and at times touch the seafloor.

3.3 Enrichment of (trace) metals compared to the ambient seawater

NMDS ordination (Fig. 4) based on Euclidean distance resemblance of normalised element / Fe molar ratio data of all collected water samples (2D stress = 0.03), revealed a clear distinction of the different samples. Most outstanding are the samples from above-plume waters, indicating that the chemical composition is different from the other samples.

The remaining samples showed less variation, nonetheless the samples collected from below the plume and the samples collected away from the main path of the plume can be distinguished. This shows that the hydrothermal plume can be characterised by its chemical composition. When comparing samples taken in the turbidity maximum of the plume to the above-plume water samples taken at 1000 m water depth it is found that Fe, Cu, P, V and Pb are enriched by factors of $\sim$ 80, $\sim$ 90, $\sim$ 17, $\sim$ 52 and $\sim$ 25, respectively. Elements with a more moderate degree of enrichment are Co, Mn, Zn, Al and Ni, with enrichment factors of $\sim$ 8.0, $\sim$ 2.5, $\sim$ 10.3, $\sim$ 1.4 and $\sim$ 1.6, respectively. The REEs were enriched by a factor of 5 to 40 relative to the clear water. U, Ti and Ca are slightly enriched at turbidity maxima, by factors of $\sim$ 1.3, $\sim$ 1.6 and $\sim$ 1.2, respectively. In and Sn are depleted compared to the above-plume water.

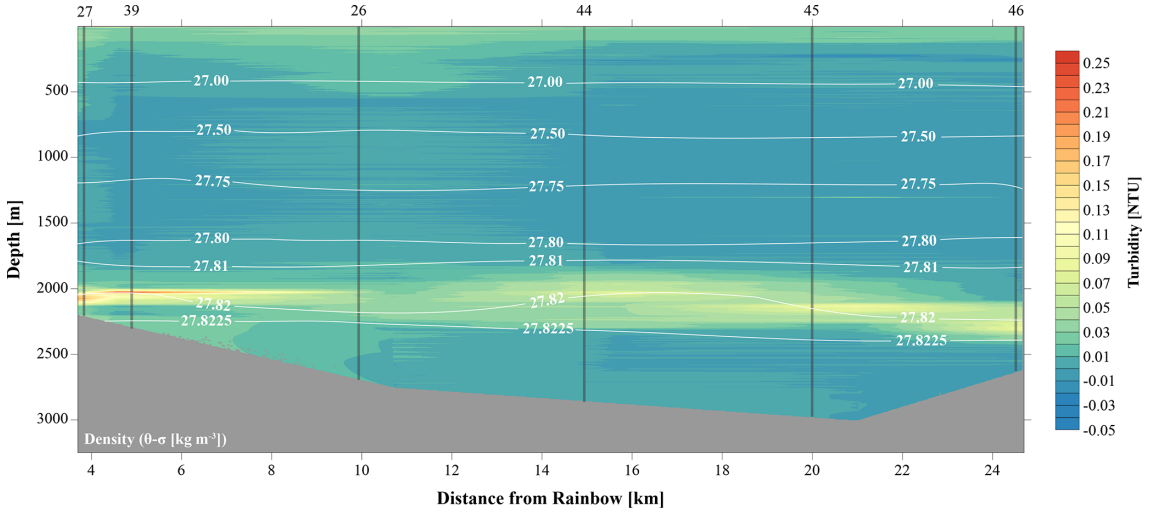

Figure 2. Transect along main plume path (indicated in Fig. 1 as plume transect), showing turbidity in the water column. The plume is indicated by highest turbidity values and disperses away from the Rainbow vent field.

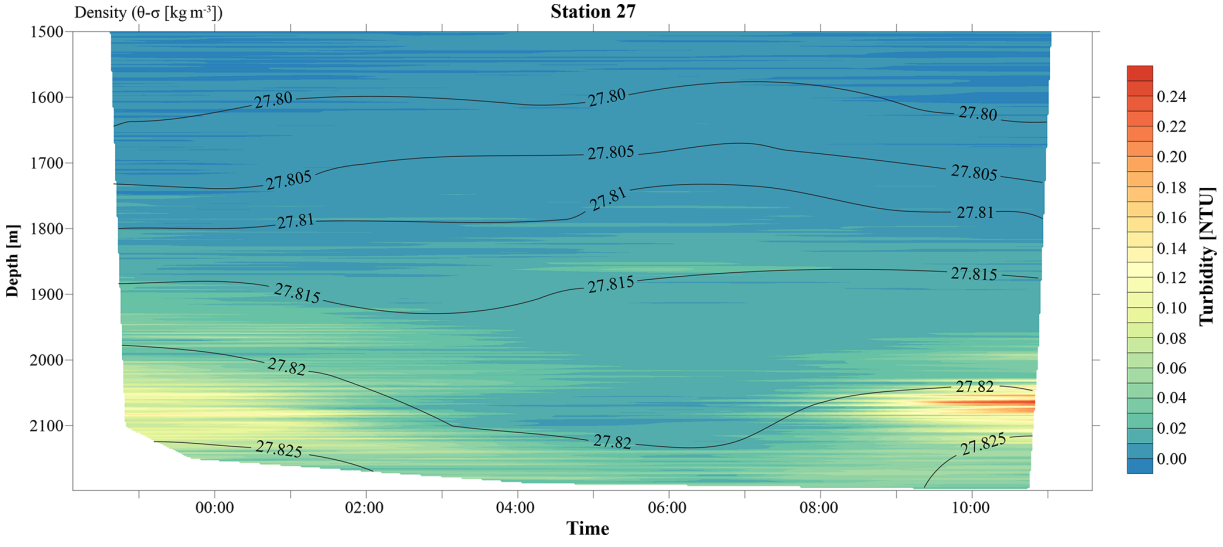

Figure 3. A 12 h yo-yo CTD at station 27 showing the temporal evolution of the hydrothermal plume over a tidal cycle.

3.4 Geochemical gradients within the hydrothermal plume

Within the hydrothermal plume, geochemical evolution is found as the plume disperses. Visual examination of the samples with the SEM, coupled with chemical analysis performed with the EDS detector, revealed that the SPM within the plume close to the Rainbow hydrothermal vent at station 32 (2.9 km north of Rainbow) mainly consisted of Fe-sulfides. In the plume samples further downstream, Fe is mainly present as Fe-oxides, Fe-hydroxides or bound in aluminosilicates.

Chemical examination of the samples showed gradients in the element / Fe molar ratios along the path of the plume, as well as off the main path of the plume at the upstream and the most distal downstream stations. Since the Fe concentration is linearly related to the turbidity (Fig. 5) ($R^2 = 0.9356$, $P < 0.001$), normalisation to Fe reveals relative enrichments or depletion of common elements. The chalcophile elements Co, Cu and Zn show a partly linear relation steepening with increasing Fe concentration (Fig. 6a for Cu), indicating that the element / Fe molar ratios are elevated close to the source but decrease towards the more distal sites (Fig. 7a). One exception is the Zn / Fe molar ratio, which is elevated at station 37, 39 and 44. Furthermore, a high Zn / Fe molar ratio is observed at upstream station 40. The oxyanions P and V are linearly related to Fe (Fig. 6b for V) and show varying element / Fe molar ratios without a clear trend of increasing or

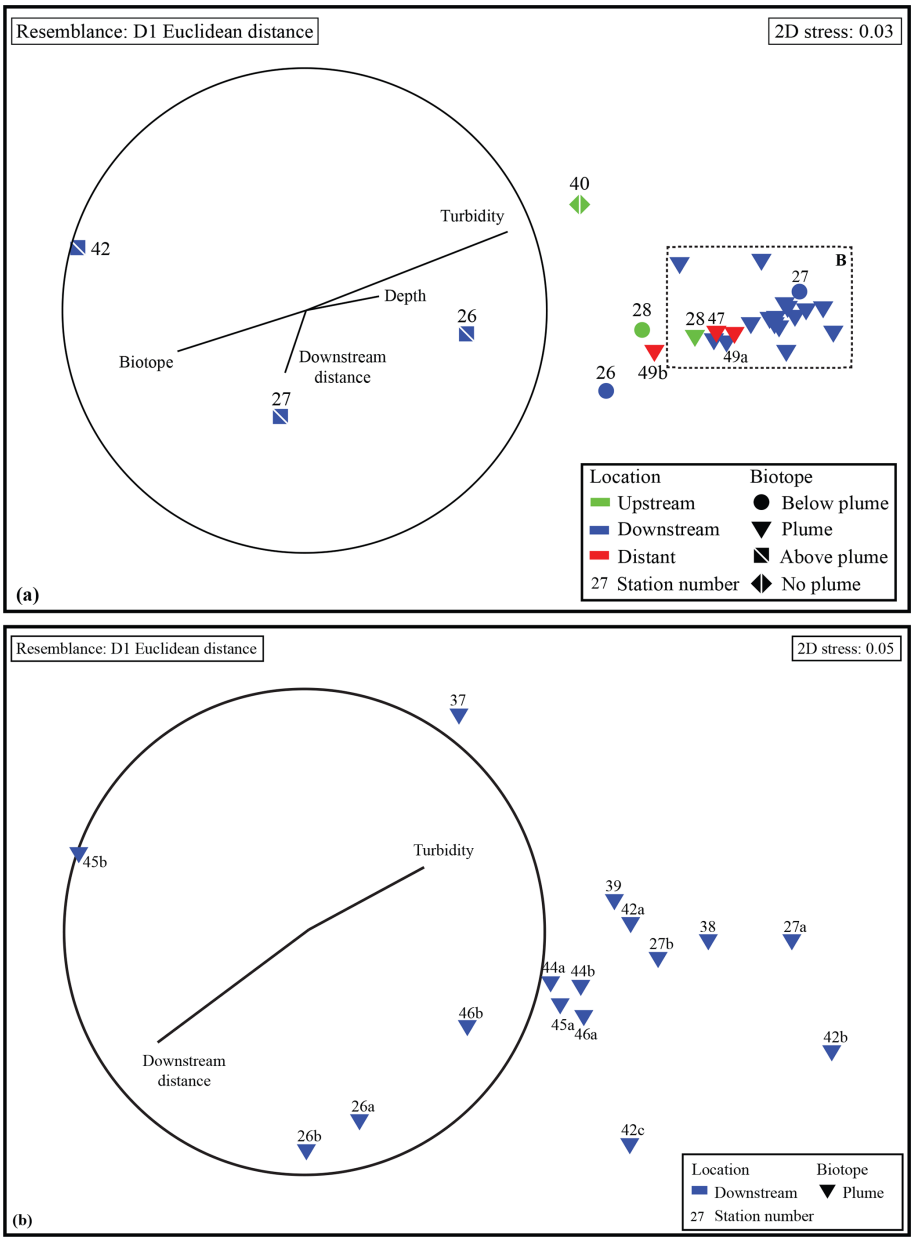

Figure 4. **(a)** NMDS ordination showing all water samples based on their resemblance in chemical composition. **(b)** NMDS ordination showing all plume samples from the downstream stations based on their resemblance in chemical composition.

decreasing ratios, both upstream and downstream of Rainbow (Fig. 7b). The REEs show a partly linear relation, levelling off with increasing Fe concentrations (Fig. 6c for Y). Within the plume this is displayed as increasing element / Fe molar ratios towards station 44, with station 42 as an exception, followed by slightly decreasing molar ratios from station 44 onwards (Fig. 7c). The Ca / Fe molar ratios ranged between 0 and 15 for most of the downstream stations, apart from the stations further downstream (47 and 49), which displayed slightly higher Ca / Fe molar ratios. Upstream station 28 had a Ca / Fe molar ratio similar to those found at station 47 and 49, and upstream station 40 was found to have a significantly higher Ca / Fe molar ratio (Fig. 7e). Other analysed elements, Mn, Al, Ni, In, Pb, Sn, Ti and U, showed no clear relationship with the Fe concentration (Fig. 6d for Sn). However, within the plume it was found that the Mn / Fe molar ratio is lower than at the upstream stations or the more distal downstream stations.

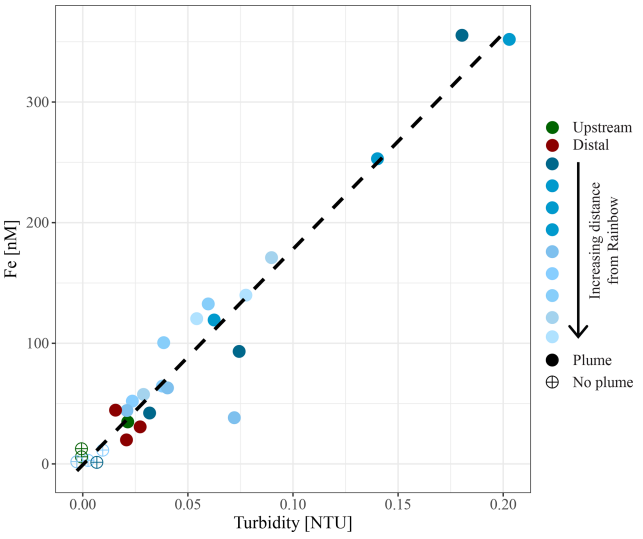

Figure 5. Relationship between in situ measured turbidity and molar concentration of particulate iron.

3.5 Microbial assemblages in water column biotopes

Samples from sediment, near-bottom water and no plume water contained microbial communities that clustered distinctly from each other and from plume, below-plume and above-plume communities (Fig. 8). In particular, sediment, near-bottom water and no plume (station 13) samples have communities that are very dissimilar from the overlying water column samples. Sediment samples appeared to cluster in a straight line, suggesting some sort of gradient of similarity along the ordination axis, though no apparent patterns were observed when independently plotted. The near-bottom water samples were relatively dispersed in the NMDS plot, suggesting a more variable community. Samples taken at the upstream station 13 from below-plume and plume depths showed no similarity with samples from corresponding depths in the other stations, whilst the above-plume community at this station is consistent with that of other stations. In general, plume and below-plume communities were more similar nearer to the vent source, with stations further downstream displaying greater dissimilarity (Figs. 9, S3).

Group average cluster analysis showed a high level of dissimilarity, i.e. large community variation, between and within biotopes. ANOSIM revealed all putative biotopes that were sampled had distinct communities (global $R = 0.738$; $P < 0.001$; 999 permutations), except for plume and below-plume samples, which could not be distinguished statistically (global $R = -0.091$; $P = 0.861$). The two seemingly unique samples from station 13 also tested as significantly distinct but with a low number of permutations (< 999) due to low replication ($n = 2$).

3.6 Univariate biodiversity

Plume and below-plume samples were less diverse than sediment samples, whilst diversity in the plume was lower than in near-bottom water samples (Kruskal–Wallis: $\chi 2 (4) = 36.127$, $P < 0.01$). In general, plume diversity was low (Fig. 10), but further differences were not statistically significant, likely due to limited replication and intra-biotope variation.

The plume microbial community at sites upstream of Rainbow and at the immediate downstream sites (stations 28, 13, 16 and 27) showed similar and relatively high biodiversity (> 4.5) (Fig. 11). Plume biodiversity at the sites further away from Rainbow gradually decreased until station 46, which displayed the lowest Shannon–Wiener index value of 2.4. Distant stations 47 and 49, showed biodiversity rising to a more moderate index value around 3.5.

3.7 Species composition

Results of the SIMPER analyses, showing the contributions of taxa composition to similarities within biotopes (Table 3), mirrored the NMDS and ANOSIM results, whereby the similarity of community composition in each biotope was dominated by a different makeup of the microbial community. The archaeal class Nitrososphaeria (marine group 1 archaea) contributed the most to similarity within the above- and below-plume water communities, while also being very common in all water samples. Alphaproteobacteria, Gammaproteobacteria and Deltaproteobacteria also constituted a large amount of the makeup of all biotopes in the area. The class Epsilonproteobacteria were rare in above-plume samples and only contributed $< 2\,\%$ to near-bottom water communities. By contrast, Epsilonproteobacteria were dominant in plume water samples (accounting for $> 35\,\%$ of the community) and were the fifth most dominant taxon in below-plume water samples contributing 8.9 % of the community.

Epsilonproteobacteria accounted for about 20 % of the plume community at stations near the vent. Beyond the near vent stations, an increase in relative abundance of Epsilonproteobacteria with distance from the vent was observed, accounting for 64 % of the community at the distant station 46 (Fig. 12). Alphaproteobacteria, Deltaproteobacteria and Gammaproteobacteria appeared to become less dominant with distance from the plume source (Fig. 12). The communities at distant stations 47 and 49 were less dominated by Epsilonproteobacteria (around 40 %). Below-plume communities were dominated mostly by Nitrososphaeria (marine group 1 archaea), whereby Nitrososphaeria became more dominant with distance from the plume source similar to the Epsilonproteobacteria in the plume. Correlations between environmental variables (elemental chemistry and physical properties) and all microbial classes observed in the plume were evident and appeared to be class-specific (Fig. S4). The hierarchical clustering revealed eight broad response groups,

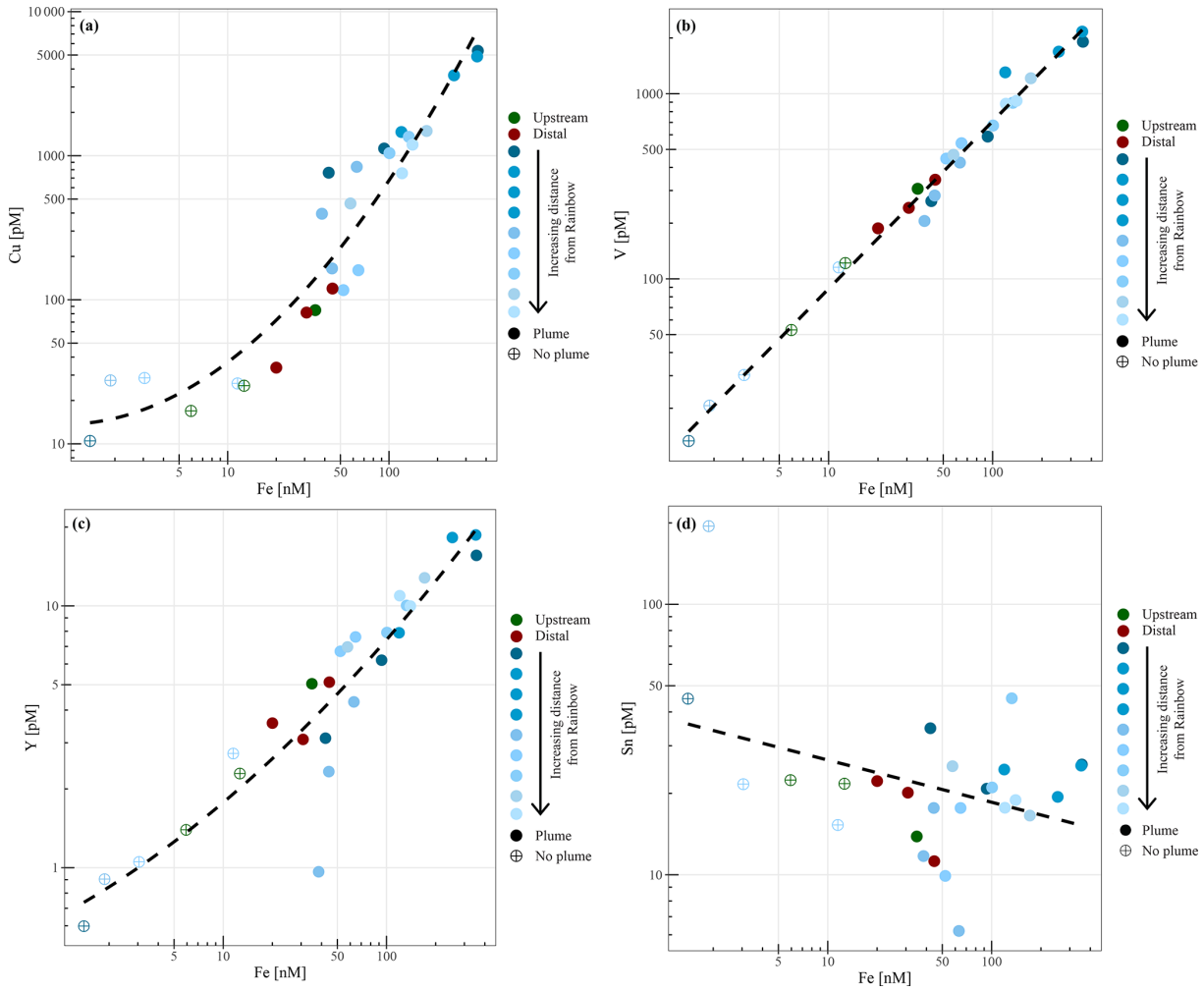

Figure 6. Relationships between molar concentrations of particulate copper **(a)**, vanadium **(b)**, yttrium **(c)** and tin **(d)** to iron.

which displayed different relationships with the environmental variables.

4 Discussion

Using a multidisciplinary approach in which physical, geochemical and ecological data were collected from the Rainbow vent neutrally buoyant plume and its underlying sediment, we aimed to expand knowledge and characteristics of the background (i.e. before impact) state of a hydrothermal vent site. Such knowledge is deemed essential to be able to assess (potential) impacts of future deep-sea SMS mining, as it may help in characterising the behaviour of the diluted distal part of chemically enriched mining plumes. We found geochemical and microbial differences between the above-plume, plume, below-plume and no-plume water, and, in addition, pertinent chemical and biological gradients within the extensive Rainbow hydrothermal vent plume were evident.

4.1 Physical constraints of plume location and behaviour

The plume was observed within the NADW mass, constrained to an isopycnal density envelope of 27.82 kg m^{-3} (Figs. 2 and 3). The apparent continuity of this turbid water layer, especially to the northeast of the Rainbow field, and lack of similarly turbid waters in the bottom waters below the plume, link the plume to Rainbow and preclude local sediment resuspension as an origin. Using turbidity measurements and presumed plume path, we traced the plume up to 25 km away from the vent source. This is within the range mentioned by German et al. (1998), who found that the Rainbow plume extends over 50 km, being controlled by local hydrodynamics and topography. Unexpectedly, in the basin upstream of the Rainbow vent field, a turbidity peak at 1975 m water depth resembling a plume was observed as well (station 28), confounding our assumption of a clear water column at upstream stations and distant downstream stations. This suggests that the plume is distributed much fur-

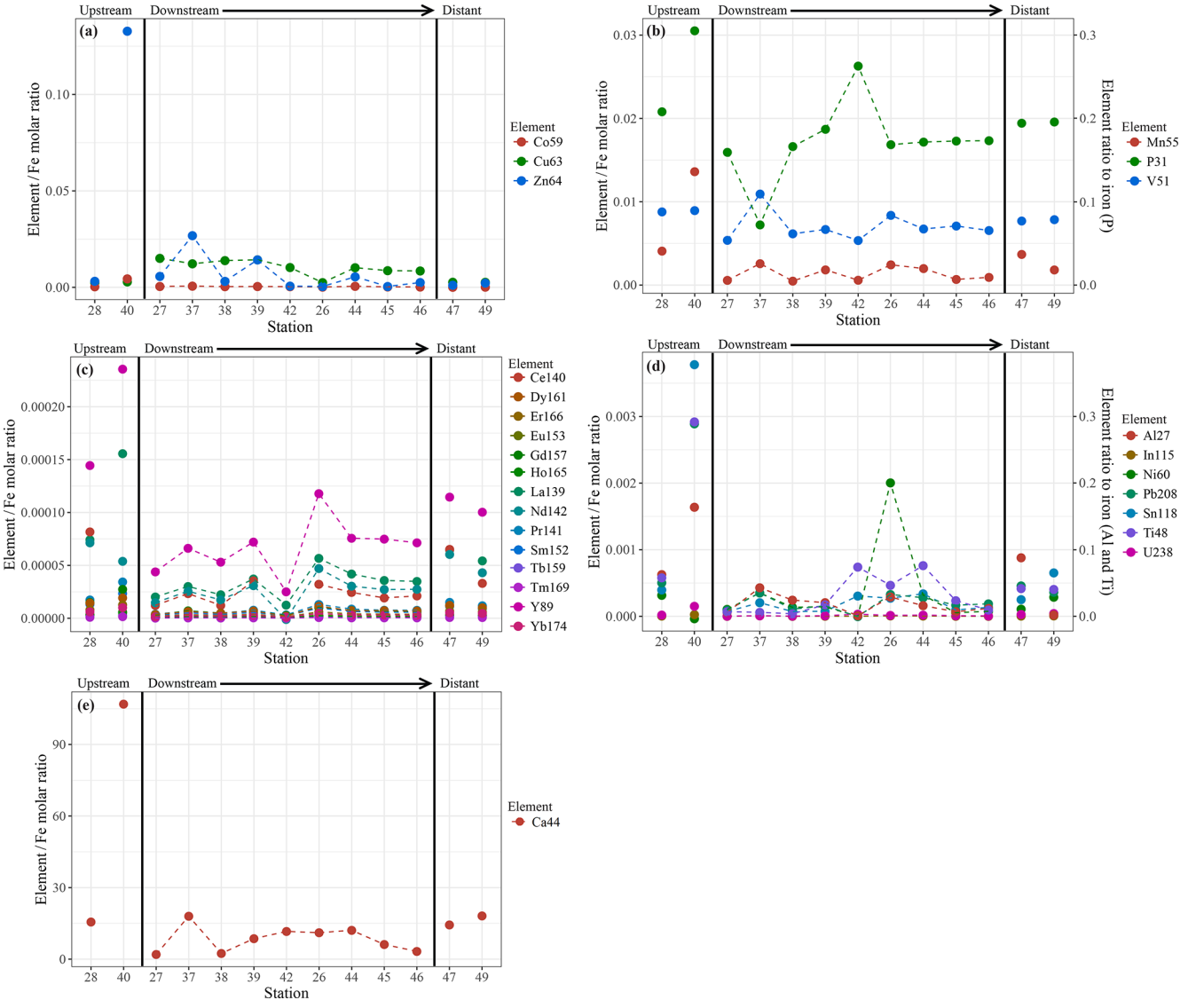

Figure 7. Element to iron molar ratios of plume samples of upstream, downstream and distant stations. Downstream stations follow the main path of the plume. **(a)** shows the element / Fe molar ratios of the chalcophiles (Co, Cu and Zn), **(b)** shows the ratios of Mn and the oxyanions (P and V), **(c)** displays the ratios of REEs, **(d)** the ratios of Al, In, Ni, Pb, Sn, Ti and U and **(e)** shows the Ca / Fe molar ratios.

ther than previously observed by Thurnherr and Richards (2001) and German et al. (1998). This is exemplified by the local variation in microbial community composition of upstream stations (Fig. 12) and is supported by the relatively low Ca / Fe molar ratio at station 28 (Fig. 7), indicating hydrothermal influence. In addition, the observed variability of plume strength and vertical position (Fig. 3) indicate that local fluctuation in the current regime and tidal motions influence plume behaviour. This dynamic behaviour has implications for survey designs and should be considered when monitoring natural and man-made plumes, such as mining-related plumes. Prior insight into plume extension and behaviour is required for the identification of adequate control sites and for tracking of plume evolution in future impact studies.

4.2 Plumes influence on the water column chemical and microbial make-up

The neutrally buoyant plume introduced pelagic heterogeneity in terms of chemical and microbial composition, which is supported by the vertical classification of the different biotopes. The neutrally buoyant plume was evidently enriched in metals and REEs compared to overlying clear water. Element concentrations were found to be in line with those found by German et al. (1991) and Edmond et al. (1995) and Edmonds and German (2004), who studied the Trans-Atlantic Geotraverse (TAG) hydrothermal plume and the Rainbow hydrothermal plume, respectively. Our chemical results from Rainbow also match with those of Lud-

Table 3. SIMPER similarity results of each biotope at class level.

Biotope	Average similarity (%)	Class	Average proportion (%)	Average similarity	Sim/SD	Contribution (%)	Cumulative (%)
Above plume	82.34	Nitrososphaeria	27.10	22.79	4.61	27.67	27.67
		Alphaproteobacteria	18.34	15.22	4.15	18.49	46.16
		Gammaproteobacteria	13.44	11.58	5.52	14.07	60.23
		Deltaproteobacteria	10.67	8.46	3.38	10.27	70.50
		Marinimicrobia (SAR406 clade)*	8.22	6.96	6.07	8.46	78.96
		Dehalococcoidia	6.38	5.69	9.19	6.91	85.87
		Thermoplasmata	2.63	2.26	5.68	2.74	88.61
		Acidimicrobiia	2.13	1.89	8.62	2.30	90.91
Plume	76.74	Epsilonproteobacteria	39.59	30.29	2.53	39.47	39.47
		Nitrososphaeria	12.16	10.32	4.05	13.45	52.92
		Gammaproteobacteria	9.69	7.92	4.71	10.32	63.23
		Alphaproteobacteria	9.23	7.22	2.44	9.40	72.64
		Deltaproteobacteria	7.60	5.56	2.75	7.25	79.88
		Dehalococcoidia	4.57	3.55	2.58	4.63	84.51
		Marinimicrobia (SAR406 clade)*	4.02	3.07	3.83	4.00	88.51
		Thermoplasmata	2.56	1.94	3.39	2.53	91.04
Below-plume	77.94	Nitrososphaeria	22.35	16.60	3.29	21.30	21.30
		Alphaproteobacteria	13.26	11.43	5.18	14.67	35.97
		Deltaproteobacteria	10.88	9.25	8.31	11.87	47.84
		Gammaproteobacteria	10.60	8.89	7.78	11.40	59.24
		Epsilonproteobacteria	9.65	7.18	2.50	9.22	68.46
		Dehalococcoidia	7.84	6.97	7.89	8.95	77.40
		Marinimicrobia (SAR406 clade)*	6.32	4.49	2.31	5.76	83.16
		Thermoplasmata	4.69	3.04	2.20	3.90	87.07
		Phycisphaerae	1.97	1.75	7.60	2.24	89.31
		Planctomycetacia	2.03	1.50	2.96	1.93	91.23
Near-bottom water	75.71	Gammaproteobacteria	20.79	16.77	3.18	22.15	22.15
		Nitrososphaeria	16.90	13.54	3.79	17.89	40.04
		Alphaproteobacteria	15.55	13.25	5.47	17.50	57.54
		Deltaproteobacteria	6.68	5.89	5.99	7.78	65.32
		Oxyphotobacteria	5.93	4.04	2.18	5.34	70.66
		Dehalococcoidia	4.08	2.99	2.50	3.95	74.61
		Phycisphaerae	3.72	2.57	2.03	3.40	78.01
		Thermoplasmata	2.47	1.70	2.25	2.24	80.25
		Acidimicrobiia	2.06	1.61	2.72	2.13	82.38
		Bacteroidia	2.15	1.57	1.85	2.07	84.45
		Marinimicrobia (SAR406 clade)*	1.75	1.24	2.17	1.64	86.09
		OM190	1.64	1.14	2.02	1.51	87.60
		Planctomycetacia	1.40	1.09	2.76	1.44	89.04
		Epsilonproteobacteria	1.71	0.85	1.08	1.12	90.16
Sediment	82.51	Gammaproteobacteria	29.67	27.17	8.51	32.93	32.93
		Alphaproteobacteria	13.98	12.44	4.88	15.07	48.01
		Deltaproteobacteria	11.98	10.98	10.24	13.30	61.31
		Nitrososphaeria	7.73	5.69	3.74	6.90	68.21
		Phycisphaerae	5.46	5.01	7.85	6.07	74.28
		Dehalococcoidia	3.35	2.48	2.58	3.01	77.29
		BD2-11 terrestrial group	2.36	1.91	2.90	2.31	79.60
		Subgroup 22 (Acidobacteria)	2.10	1.74	3.22	2.11	81.71
		OM190	2.09	1.50	5.50	1.81	83.53
		Nitrospira	1.79	1.49	3.68	1.80	85.33
		Bacteroidia	1.91	1.48	3.66	1.79	87.12
		Acidimicrobiia	1.58	1.24	2.84	1.50	88.62
		Thermoanaerobaculia	1.41	1.07	3.25	1.30	89.92
		Gemmatimonadetes*	1.57	1.06	1.56	1.28	91.21

* Indicates undefined class.

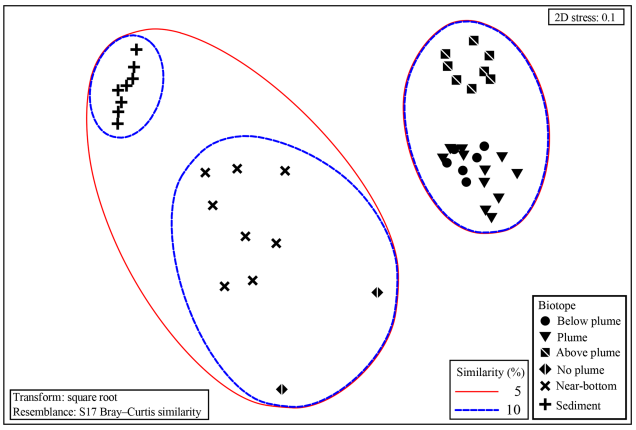

Figure 8. Non-metric multidimensional scaling plot of the microbial community composition of all samples based on Operational Taxonomic units. Similarity groupings are based on group average clustering. "No plume" is representative of samples collected from station 13, where there was no indication of a plume.

ford et al. (1996), who studied vent fluid samples from the TAG, Mid-Atlantic Ridge at Kane (MARK), Lucky Strike and Broken Spur vent sites; i.e. our element concentrations were found to be in the same order of magnitude as theirs (Table S2).

The distinctive chemical composition of the plume samples (e.g. metal concentrations) affects chemolithoautotrophic microbial growth within the plume, as indicated by the typical microbial community in plume samples. We observed a clear and consistent separation between communities in the plume and those in above-plume samples. The influence of MOW on the above-plume community could also play a role, as water masses can harbour different microbial communities (Agogue et al., 2011). However, the palpable presence of a plume in the turbidity data with supporting chemical measurements and the occurrence of vent-associated Epsilonproteobacteria (Olins et al., 2017; Djurhuus et al., 2017) and other vent-associated groups, such as the Gammaproteobacteria clade SUP05 (Sunamura et al., 2004), point to a unique chemical environment. Here chemosynthetic communities flourish and give rise to independent biotopes in the neutrally buoyant plume kilometres downstream of the vent site.

Below-plume communities were not distinct from the plume biotope, although instead of Epsilonproteobacteria, the ubiquitous class Nitrososphaeria was the most dominant group, reflecting some similarities with above-plume seawater communities. Similarities between plume and proximal habitat communities have also been observed by Olins et al. (2017), whereby intra-field (defined as within vent field between diffuse flows) and diffuse flow microbial communities were alike. In our study, similarities between plume and below-plume water are likely derived from precipitation of mineral and microbial aggregates dragging plume microbes deeper below the plume, as suggested by Dick et al. (2013). In addition, internal wave-induced turbulence causes vertical mixing along the slope of the Rainbow Ridge (van Haren et al., 2017), which may cause the plume and associated communities near the vent field to mix with ambient water communities, leading to assemblage similarities. This indicates the plume and that associated microbial processes could have a larger vertical footprint than previously observed, supporting suggestions by Olins et al. (2017) that proximal non-plume habitats have been overlooked. Interestingly, near-bottom water (and sediment) community assemblages were distinct from the below-plume and other water column communities. This could imply (1) that there is little "fallout" from the plume at distance from the vent, which is in agreement with sediment trap observations by Khripounoff et al. (2001); that (2) plume-specific bacteria die off due to lack of energy sources and DNA degrades before reaching the seafloor; and that (3) microbes are more abundant in the near-bottom waters, either naturally or through mechanical disturbance resuspending sediment during the coring process, outnumbering groups that have been mixed in from overlaying water. Despite the presence of a plume and precipitation, a difference between the sea floor and the water column biotopes is present, consistent with global broadscale non-vent benthic–pelagic patterns (Zinger et al., 2011). According to Khripounoff et al. (2001), particulate fallout from the Rainbow plume is spatially very limited. This implies that the extended chemical imprint on the sediment (reported by Cave et al. , 2002; Chavagnac et al. , 2005; and this study) is likely to have formed when the plume is in direct contact with the sediment during its vertical tidal migration. As the plume rises again, the associated distinct communities apparently resume dominance in the near-bottom water. Though Epsilonproteobacteria have been detected in Rainbow vent sediments comprising over 5 % of the sediment community (López-García et al., 2003), very few reads of this group in sediment samples were present in our study, probably as our coring samples were collected kilometres away from the venting site. Cave et al. (2002), observed chemical evolution of sediment composition with distance from source, thus we infer a relationship between the sediment dwelling Epsilonproteobacteria with nearby plume precipitates, such as Cu and presumed precipitates Zn and Cd (Trocine and Trefry, 1988). Additionally, extracellular DNA degradation rate can be 7 to 100 times higher in sediment than in the water column (Dell'Anno and Corinaldesi, 2004). Therefore, although our results suggest no microbial plume community imprint on the sediment, we cannot rule out short-lived episodic community changes when the plume is in contact with the sediment.

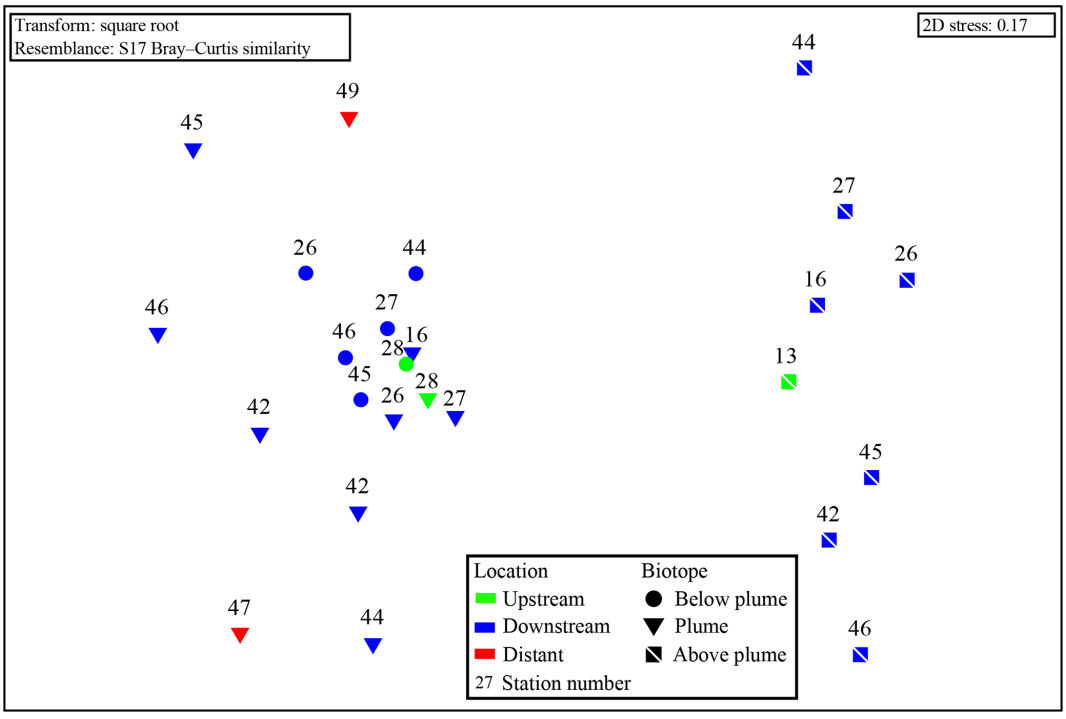

Figure 9. Non-metric multidimensional scaling plot of the microbial community composition of all water column samples based on Operational Taxonomic units. Plume and below-plume depths from Station 13 were excluded.

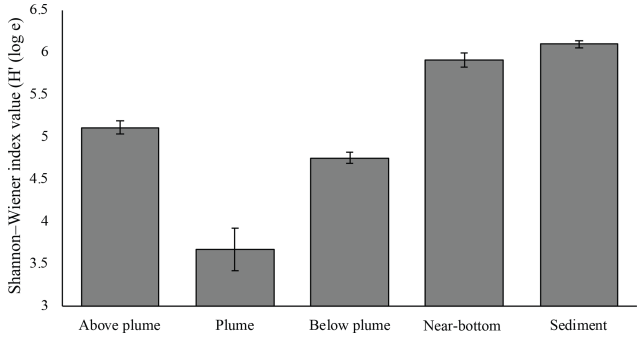

Figure 10. Mean Shannon–Wiener diversity index for microorganisms in each biotope. Error bars represent ± SE.

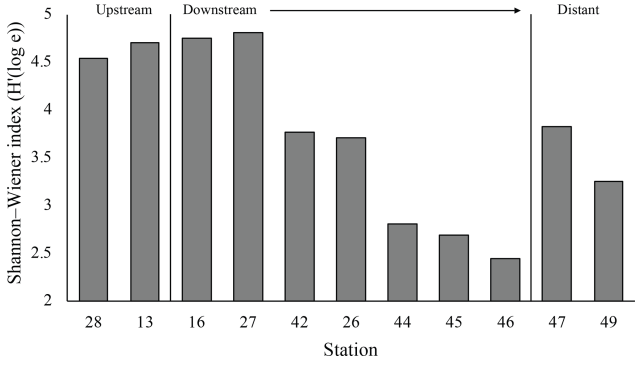

Figure 11. Shannon–Wiener index values for microorganisms in each plume sample taken.

4.3 Geochemical gradients within the hydrothermal plume

Analysis of SPM in water samples taken along the flow path of the plume, as well as off the flow path, showed conspicuous trends of elements, reflecting the chemical evolution of the plume as it drifts away from its hydrothermal source.

The chalcophile elements (Cu, Co and Zn) were found to have the highest element / Fe molar ratios closest to the vent site, indicating either rapid removal from the hydrothermal plume or removal from the solid phase as the plume drifts away from the vent site. Using SEM-EDS, it was demonstrated that at the proximal downstream stations mainly Fe-sulfides were found, whereas Fe-(oxyhydr)oxides were found further downstream. This suggests that chalcophile elements are mainly present in the form of sulfide mineral particles at the proximal stations, which are entrained in the flow of hydrothermal water emanating from the Rainbow vents. Subsequently, they are rapidly lost by settling from the plume in sulfide-bearing phases, while a large portion of Fe remains in suspension (Cave et al., 2002; Edmonds and German, 2004), consistent with decreasing concentrations of Cu, Zn and Co in sediment recovered from the Rainbow area with increasing distance to the vent site (Cave et al., 2002).

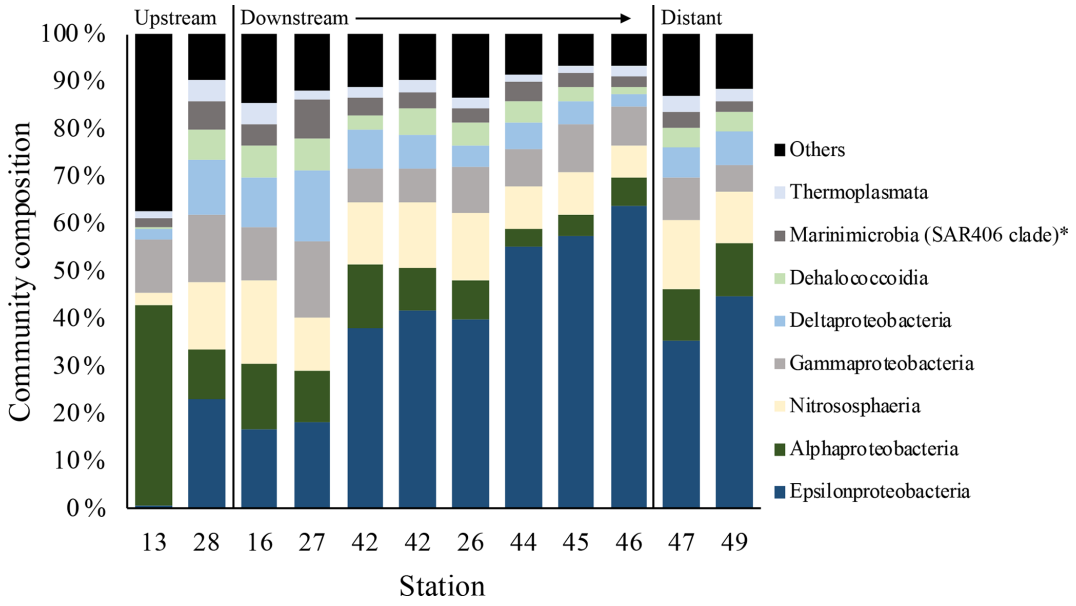

Figure 12. Microbial community composition in the plume samples as a percentage of the dominant class groups in accordance with the SIMPER results. The asterisk indicates an undefined class.

The oxyanions (V and P) showed slightly varying element / Fe molar ratios with increasing distance away from Rainbow, suggesting co-precipitation with Fe as oxyhydroxides (Edmonds and German, 2004). No additional uptake of these elements was observed with increasing distance from the vent field (German et al., 1991), since these elements are scavenged initially in significant amounts during the buoyant plume phase (Cave et al., 2002).

The trend shown by Mn / Fe molar ratios can be attributed to the slower oxidation kinetics of Mn (Cave et al., 2002). It takes longer for reduced Mn to be oxidised than it would for Fe, resulting in an increase in particulate Mn with increasing distance from the Rainbow hydrothermal vent field, which subsequently settles out from the plume as Mn-oxyhydroxides (Cave et al., 2002).

The observed positive relationship between the REEs and Fe is indicative of continuous scavenging of these elements from the ambient seawater onto Fe-oxyhydroxides (Edmonds and German, 2004; Chavagnac et al., 2005; Caetano et al., 2013). Therefore, the highest element / Fe molar ratios were observed away from the Rainbow hydrothermal vent site, where Fe-(oxyhydr)oxides are dominant more distal to the vent site.

The Ca / Fe molar ratios vary between 0 and 15 for the stations downstream of the Rainbow hydrothermal vent but are higher at the distant downstream station 47 and 49 and upstream stations 28 and 40. Especially at station 40, located on the Rainbow Ridge, the Ca / Fe molar ratio is significantly higher than at the other stations. This is in line with observations by Khripounoff et al. (2001) and Cave et al. (2002), who also found that the relative Ca concentration in settling particles and the sediments is lower close the Rainbow vent field and increases as the Fe concentration decreases when the plume disperses. Since Ca is naturally present in high abundances in pelagic skeletal carbonate that rains down from the overlying water column and Fe is mainly present as a hydrothermal component, the Ca / Fe molar ratio could be an indicator for the extent of the hydrothermal influence. The high molar ratio at station 40 would then suggest that this station is hardly or not at all influenced by the hydrothermal plume, as the natural abundance of particulate iron is low (e.g. Michard et al., 1984 and this study), whereas stations 28, 47 and 49 are, as expected, influenced in more moderate degrees compared to the stations directly downstream of Rainbow.

4.4 Microbial gradients within the hydrothermal plume

The microbial plume community composition and diversity altered with distance from the plume source, showcasing horizontal heterogeneity within the plume. Despite dilution, the vent-associated group Epsilonproteobacteria (specifically the most common genus *Sulfurimonas*), appeared to dominate the community composition. This is likely due to its flexibility to exploit a range of electron donors and acceptors (Nakagawa et al., 2005), making them suitable inhabitants of dynamic environments (Huber et al., 2003). From the relative abundance data presented here it cannot be determined whether Epsilonproteobacteria dominate by rapid reproduction or if other groups decline in abundance. However, it is evident that Epsilonproteobacteria remain competitive or outcompete other competitors, such as gener-

alist Gammaproteobacteria that are often vent associated (i.e. SUP05). It is unlikely that this pattern is caused by entrainment of Epsilonproteobacteria from background seawater over time. This is based on the lack of significant presence of Epsilonproteobacteria in above-plume water and at remote station 13 and reduced mixing that neutrally buoyant plumes generally experience (McCollom, 2000). This is further supported by the increasing uniqueness of the plume community with distance from the source, suggesting that mixing and entrainment between downstream biotopes is negligible.

The neutrally buoyant plume is likely too chemically enriched for non-adapted microbial taxa to thrive and consequently they are outcompeted by groups that can benefit from or tolerate the chemical nature of the plume. Therefore, it is likely that less specialised groups die out due to lack of appropriate resources and interspecies competition, as indicated by the decline in biodiversity with age of plume (distance) directly mirroring the increasing dominance of Epsilonproteobacteria, a group already known to influence diversity and community structures (Opatkiewicz et al., 2009; Sylvan et al., 2012). In addition, the decrease in concentration of particulate matter may influence microbial diversity (Huber et al., 2003). Temporal succession has been observed within plume environments by Sylvan et al. (2012) and Reed et al. (2015), driven by metabolic energy yield and concentration of the electron donors. These patterns may relate to ecological succession (Connell and Slaytor, 1977) within the plume with change in microbial communities resulting in a low diversity climax plume community. At the distant stations 47 and 49, the community was less dominated by Epsilonproteobacteria and more diverse, indicating a gradual return to what is possibly a non-plume-influenced state of the microbial community. The wide range of correlations within and between microbial classes and water properties, i.e. ranging from chemical to physical variables (Fig. S4), indicates a complex array of community drivers within the plume.

In contrast to our results, Sheik et al. (2015) and Djurhuus et al. (2017) observed decreasing Epsilonproteobacteria abundance within hundreds of metres from the source in the rising, buoyant portion of plumes generated by Indian Ocean and South Pacific Ocean vents. Interestingly, in our results Epsilonproteobacteria were least dominant in the neutrally buoyant plume closest to the Rainbow vent site, which may indicate that entrainment of other microbial groups within the rising portion of the plume initially dilutes the contribution of Epsilonproteobacteria (possibly derived from near seafloor communities), whilst the competitive advantage of certain species from this group only becomes evident at a later stage as the plume drifts away from the source. However, Huber et al. (2003) suggested that Epsilonproteobacteria thrive in hydrothermal fluid mixed with seawater due to the lower temperature and high electron acceptor availability, suggesting greater habitat suitability away from the immediate venting orifice. Furthermore, it has been demonstrated that Epsilonproteobacteria (specifically *Sulfurimonas*) have higher dispersal capabilities than thermophilic vent-associated microbial groups (Mino et al., 2017). A sampling design to follow the continuity of the plume from the buoyant to the neutrally buoyant portion would be a suitable approach to fully trace the evolution of the plume from the orifice to full dilution. However, the term full dilution is ambiguous as it is unknown exactly how far the plume influences the water properties and how far the plume-associated bacteria will follow, adding water column microbial community heterogeneity beyond our study spatial extent.

4.5 Possible effects of SMS mining plumes

Mining of SMS deposits will create additional plumes generated by activities of mining vehicles (resuspension) and by the discharge of solids from the surface vessel (discharge plume). It is yet unknown how these plumes will affect the ecosystem at active and inactive hydrothermal vent sites. Our study showed the influence of a natural hydrothermal plume on the pelagic microbial and chemical composition up to 25 km away from its source. It is not unlikely that the dispersion of sediment and chemically reactive mineral material in the water column may cause similar or larger changes to the background state.

While large particles mobilised by mining are expected to stay close to the seafloor and settle out rapidly, smothering fauna in the immediate surroundings (Jones et al., 2018), smaller particles will disperse further, potentially invoking effects on a larger spatial scale. Modelling the behaviour of the discharge plume generated by the proposed Solwara 1 SMS mining has shown that these plumes can extend up to 10 km from the mining site, resulting in a deposit thickness of up to 50 cm within 1 km of the discharge site (Gwyther et al., 2008; Boschen et al., 2013). Apart from the physical impact that suspended fine-grained solids may have, especially on suspension feeders, the presence of chemically reactive material may give the mining plume a distinct chemical and microbial fingerprint, analogous in a certain context to what we observed in the natural plume.

The extent of the local impact of deep-sea mining will depend on the location where the mining takes place. At an active site like the Rainbow hydrothermal vent field, we showed that even in the distant plume (25 km away from Rainbow) hydrothermal plume microbiota dominate. When a mining discharge plume at an active hydrothermal vent field would be merged with the natural plume, the local effects might be minimal since microbial communities are already adapted to the metal-rich environments (Gwyther et al., 2008). However, a mining plume consisting of a dense suspension of bottom sediment and fine-grained metal sulfides is expected to support an altered microbial community in terms of abundance and composition, impacting the hydrothermal plume community. Moreover, the effects over larger spatial scales could be multiplied because of the increased export of electron donors by mining activities. Reed et al. (2015), who

studied a hydrothermal plume in the Lau Basin, have shown that the export of the chemolithoautotrophs from a plume increases with increasing availability of electron donors. Dispersion of chemolithoautotrophs is variable between groups depending on the energetics of their metabolisms; for example, methanotrophs that can disperse more than 50 km are likely to disperse further than sulfur oxidisers (Reed et al., 2015). Increased export of microbial biomass from plumes may have an impact on other marine systems that are hospitable to chemolithoautotrophs, such as oxygen minimum zones (Dick et al., 2013), and to higher trophic levels (Phillips, 2017). At inactive sites the effect on the background fauna is also potentially large since these are not adapted to the heavy-metal-rich environments and the discharge plume could prove to be toxic to the fauna (Boschen et al., 2013), possibly affecting organisms at all levels of the food chain (Weaver et al., 2018). In addition, in cases of multiple plumes at different depths due to stratification and vertical migration due to tidal regimes, the impacts may not be confined to a single depth band and may affect a large part of the water column, including other habitats, such as benthic habitats (Klunder et al., 2020).

5 Conclusions

Our results demonstrate that geochemically enriched plumes provide a dynamic habitat that is conducive to ecological changes over a short time span. Combining microbial and chemical analysis has proven to be a sensitive tool, which enabled us to trace the hydrothermal plume up to 25 km downstream from the vent source and also upstream of the Rainbow vent site, implying that the influence of the hydrothermal vent on the surrounding environment may reach further than previously thought. The neutrally buoyant plume was chemically enriched, which spawned a distinct microbial biotope dominated by vent-associated species. As the plume aged and dispersed, we observed alteration of the chemical composition and microbial community composition of the plume, showcasing a horizontal heterogeneous plume. Overall we have shown that a hydrothermal plume acts as a unique chemically enriched environment where distinct and variable microbial habitats are present. The plume heterogeneity and its dynamical behaviour would require extensive sampling in order to be able to assess the impacts and interferences by man-made mining plumes on the natural conditions.

Data availability. CTD data presented in this work; filter weights for SPM sampling, geochemical data of the (trace) metals, and REEs; associated calculated enrichment factors and information on the blanks; drift measurements; and detection limits of the SF-ICP-MS analyses are available in the NIOZ data portal (https://dataverse.nioz.nl/dataverse/doi under DOI https://doi.org/10.25850/nioz/7b.b.s, Haalboom and De Stigter, 2019, last access: 26 November 2019) and are also submitted to PANGAEA. Raw sequence data are available via the European Nucleotide Archive (ENA), under accession number PRJEB36848.

Supplement. The supplement related to this article is available online at: https://doi.org/10.5194/bg-17-2499-2020-supplement.

Author contributions. GD, HDS and FM conceptualised the study and undertook data collection. SH and DP undertook sample processing and analysis with contributions from and under the supervision of FM, GD, GJR, HDS, JvB and HW. SH and DP wrote the manuscript with contributions from all co-authors.

Competing interests. The authors declare that they have no conflict of interest.

Acknowledgements. We thank Evaline van Weerlee for assistance in DNA extraction, Patrick Laan for assistance in the chemical analysis of the collected samples, and Hans Malschaert for maintaining the bioinformatics hardware and software tools. We also thank the crew and captain of the RV *Pelagia*, as well as the NIOZ technicians, for their essential assistance during cruise 64PE398. We thank Valérie Chavagnac and an anonymous reviewer for reviewing the paper and their collective constructive feedback.

Financial support. This research has been supported by the Applied and Engineering Sciences (AES) domain of the Netherlands Organisation for Scientific Research (NWO) (grant no. 13273) and by partners from the Dutch maritime industry. Topsector Water, a collaborative effort of Dutch industry, academia and government, funded ship time. Sabine Haalboom received funding from the Blue Nodules project (EC grant agreement no. 688785). David Price is supported by the Natural Environmental Research Council (grant no. NE/N012070/1). Henko de Stigter received funding from TREASURE. Furu Mienis is supported financially by the Innovational Research Incentives Scheme of the Netherlands Organisation for Scientific Research (NWO-VIDI grant no. 0.16.161.360).

Review statement. This paper was edited by Julia Uitz and reviewed by Valérie Chavagnac and one anonymous referee.

References

Agogue, H., Lamy, D., Neal, P. R., Sogin, M. L., and Herndl, G. J.: Water mass-specificity of bacterial communities in the North Atlantic revealed by massively parallel sequencing, Mol. Ecol., 20, 258–274, https://doi.org/10.1111/j.1365-294X.2010.04932.x, 2011.

Anantharaman, K., Breier, J. A., and Dick, G. J.: Metagenomic resolution of microbial functions in deep-sea hydrothermal plumes across the Eastern Lau Spreading Center, Isme J., 10, 225–239, https://doi.org/10.1038/ismej.2015.81, 2016.

Boschen, R. E., Rowden, A. A., Clark, M. R., and Gardner, J. P. A.: Mining of deep-sea seafloor massive sulfides: A review of the deposits, their benthic communities, impacts from mining, regulatory frameworks and management strategies, Ocean Coast. Manage., 84, 54–67, https://doi.org/10.1016/j.ocecoaman.2013.07.005, 2013.

Breier, J. A., Toner, B. M., Fakra, S. C., Marcus, M. A., White, S. N., Thurnherr, A. M., and German, C. R.: Sulfur, sulfides, oxides and organic matter aggregated in submarine hydrothermal plumes at 950′ N East Pacific Rise, Geochim. Cosmochim. Ac., 88, 216–236, https://doi.org/10.1016/j.gca.2012.04.003, 2012.

Caetano, M., Vale, C., Anes, B., Raimundo, J., Drago, T., Schimdt, S., Nogueira, M., Oliveira, A., and Prego, R.: The Condor seamount at Mid-Atlantic Ridge as a supplementary source of trace and rare earth elements to the sediments, Deep-Sea Res. Pt. II, 98, 24–37, https://doi.org/10.1016/j.dsr2.2013.01.009, 2013.

Cave, R. R., German, C. R., Thomson, J., and Nesbitt, R. W.: Fluxes to sediments underlying the Rainbow hydrothermal plume at 36°14′ N on the Mid-Atlantic Ridge, Geochim. Cosmochim. Ac., 66, 1905–1923, https://doi.org/10.1016/S0016-7037(02)00823-2, 2002.

Cerqueira, T., Barroso, C., Froufe, H., Egas, C., and Bettencourt, R.: Metagenomic Signatures of Microbial Communities in Deep-Sea Hydrothermal Sediments of Azores Vent Fields, Microb. Ecol., 76, 387–403, https://doi.org/10.1007/s00248-018-1144-x, 2018.

Charlou, J. L., Donval, J. P., Fouquet, Y., Jean-Baptiste, P., and Holm, N.: Geochemistry of high H_2 and CH_4 vent fluids issuing from ultramafic rocks at the Rainbow hydrothermal field (36°14′ N, MAR), Chem. Geol., 191, 345–359, https://doi.org/10.1016/S0009-2541(02)00134-1, 2002.

Chavagnac, V., German, C. R., Milton, J. A., and Palmer, M. R.: Sources of REE in sediment cores from the Rainbow vent site (36°14′ N, MAR), Chem. Geol., 216, 329–352, https://doi.org/10.1016/S0009-2541(02)00134-1, 2005.

Clarke, K. R. and Gorley, R. N.: PRIMER v6: User Manual/Tutorial (Plymouth Routines in Multivariate Ecological Research), PRIMER-E, Plymouth, 190 pp., 2006.

Collins, P. C., Croot, P., Carlsson, J., Colaço, A., Grehan, A., Hyeong, K., Kennedy, R., Mohn, C., Smith, S., and Yamamoto, H.: A primer for the Environmental Impact Assessment of mining at seafloor massive sulfide deposits, Mar. Policy, 42, 198–209, https://doi.org/10.1016/j.marpol.2013.01.020, 2013.

Connell, J. H. and Slayter, R. O.: Mechanisms of Succession in Natural Communities and Their Role in Community Stability and Organization, Am. Nat., 111, 1119–1144, https://doi.org/10.1086/283241, 1977.

Cowen, J. P. and Bruland, K. W.: Metal Deposits Associated with Bacteria – Implications for Fe and Mn Marine Biogeochemistry, Deep-Sea Res., 32, 253–272, https://doi.org/10.1016/0198-0149(85)90078-0, 1985.

Cowen, J. P., Massoth, G. J., and Feely, R. A.: Scavenging Rates of Dissolved Manganese in a Hydrothermal Vent Plume, Deep-Sea Res., 37, 1619–1637, https://doi.org/10.1016/0198-0149(90)90065-4, 1990.

Dell'Anno, A. and Corinaldesi, C.: Degradation and turnover of extracellular DNA in marine sediments: Ecological and methodological considerations, Appl. Environ. Microbiol., 70, 4384–4386, https://doi.org/10.1128/AEM.70.7.4384–4386.2004, 2004.

Dick, G. J., Clement, B. G., Webb, S. M., Fodrie, F. J., Bargar, J. R., and Tebo, B. M.: Enzymatic microbial Mn(II) oxidation and Mn biooxide production in the Guaymas Basin deep-sea hydrothermal plume, Geochim. Cosmochim. Ac., 73, 6517–6530, https://doi.org/10.1016/j.gca.2009.07.039, 2009.

Dick, G. J. and Tebo, B. M.: Microbial diversity and biogeochemistry of the Guaymas Basin deep-sea hydrothermal plume, Environ. Microbiol., 12, 1334–1347, https://doi.org/10.1111/j.1462-2920.2010.02177.x, 2010.

Dick, G. J., Anantharaman, K., Baker, B. J., Li, M., Reed, D. C., and Sheik, C. S.: The microbiology of deep-sea hydrothermal vent plumes: ecological and biogeographic linkages to seafloor and water column habitats, Front. Microbiol., 4, 124, https://doi.org/10.3389/fmicb.2013.00124, 2013.

Djurhuus, A., Mikalsen, S. O., Giebel, H. A., and Rogers, A. D.: Cutting through the smoke: the diversity of microorganisms in deep-sea hydrothermal plumes, Roy. Soc. Open Sci., 4, 160829, https://doi.org/10.1098/rsos.160829, 2017.

Douville, E., Charlou, J. L., Oelkers, E. H., Bienvenu, P., Colon, C. F. J., Donval, J. P., Fouquet, Y., Prieur, D., and Appriou, P.: The rainbow vent fluids (36°14′ N, MAR): the influence of ultramafic rocks and phase separation on trace metal content in Mid-Atlantic Ridge hydrothermal fluids, Chem. Geol., 184, 37–48, https://doi.org/10.1016/S0009-2541(01)00351-5, 2002.

Edmond, J. M. Campell, A. C., Palmer, M. R., Klinkhammer, G. P., German, C. R., Edmonds, H. N., Elderfield, H., Thompson, G., and Rona, P.: Time series studies of vent fluids from the TAG and MARK sites (1986, 1990) Mid-Atlantic Ridge: a new solution chemistry model and a mechanisms for Cu / Zn zonation in massive sulphide orebodies, Geol. Soc. Spec. Publ., 87, 77–86, https://doi.org/10.1144/GSL.SP.1995.087.01.07, 1995.

Edmonds, H. N. and German, C. R.: Particle geochemistry in the Rainbow hydrothermal plume, Mid-Atlantic Ridge, Geochim. Cosmochim. Ac., 68, 759–772, https://doi.org/10.1016/S0016-7037(03)00498-8, 2004.

Emery, W. J. and Meincke, J.: Global Water Masses – Summary and Review, Oceanol Acta, 9, 383–391, 1986.

Findlay, A. J., Gartman, A., Shaw, T. J., and Luther, G. W.: Trace metal concentration and partitioning in the first 1.5 m of hydrothermal vent plumes along the Mid-Atlantic Ridge: TAG, Snakepit, and Rainbow, Chem. Geol., 412, 117–131, https://doi.org/10.1016/j.chemgeo.2015.07.021, 2015.

Fouquet, Y., Barriga, F., Charlou, J. L., Elderfield, H., German, C. R., Ondréas, H., Parson, L., Radford-Knoery, J., Relvas, J., Ribeiro, A., Schultz, A., Appriou, R., Cambon, P., Costa, I., Donval, J. P., Douville, E., Landuré, J. Y., Normund, A., Pellé, H., Ponsevera, E., Riches, S., Santana, H., and Stephan, M.: Flores diving cruise with the Nautile near the Azores. First dives on the Rainbow field: hydrothermal seawater/mantle interaction, Inter Ridge News, 7, 24–28, 1998.

Frank, K. L., Rogers, D. R., Olins, H. C., Vidoudez, C., and Girguis, P. R.: Characterizing the distribution and rates of microbial sulfate reduction at Middle Valley hydrothermal vents, Isme J., 7, 1391–1401, https://doi.org/10.1038/ismej.2013.17, 2013.

German, C. R., Campbell, A. C., and Edmond, J. M.: Hydrothermal Scavenging at the Mid-Atlantic Ridge – Modification of Trace-

Element Dissolved Fluxes, Earth Planet. Sc. Lett., 107, 101–114, https://doi.org/10.1016/0012-821X(91)90047-L, 1991.

German, C. R., Klinkhammer, G. P., and Rudnicki, M. D.: The Rainbow hydrothermal plume, °14′ N, MAR, Geophys. Res. Lett., 23, 2979–2982, https://doi.org/10.1029/96GL02883, 1996.

German, C. R., Richards, K. J., Rudnicki, M. D., Lam, M. M., Charlou, J. L., and Party, F. S.: Topographic control of a dispersing hydrothermal plume, Earth Planet. Sc. Lett., 156, 267–273, https://doi.org/10.1016/S0012-821X(98)00020-X, 1998.

Gwyther, D. and Wright, M.: Environmental Impact Statement: Solwara 1, Coffey Natural Systems Pty Ltd, 47–65, 2008.

Han, Y. C., Gonnella, G., Adam, N., Schippers, A., Burkhardt, L., Kurtz, S., Schwarz-Schampera, U., Franke, H., and Perner, M.: Hydrothermal chimneys host habitat-specific microbial communities: analogues for studying the possible impact of mining seafloor massive sulfide deposits, Sci. Rep.-UK, 8, 10386, https://doi.org/10.1038/s41598-018-28613-5, 2018.

Huber, J. A., Butterfield, D. A., and Baross, J. A.: Bacterial diversity in a subseafloor habitat following a deep-sea volcanic eruption, FEMS Microbiol. Ecol., 43, 393–409, https://doi.org/10.1111/j.1574-6941.2003.tb01080.x, 2003.

Hoagland, P., Beaulieu, S., Tivey, M. A., Eggert, R. G., German, C., Glowka, L., and Lin, J.: Deep-sea mining of seafloor massive sulfides, Mar. Policy, 34, 728–732, https://doi.org/10.1016/j.marpol.2009.12.001, 2010.

Jannasch, H. W. and Mottl, M. J.: Geomicrobiology of Deep-Sea Hydrothermal Vents, Science, 229, 717–725, https:/doi.org/10.1126/science.229.4715.717, 1985.

Jones, D. O. B., Amon, D. L., and Chapman, A. S. A.: Mining Deep-Ocean Mineral Deposits: What are the Ecological Risks?, Elements, 14, 325–330, https://doi.org/10.2138/gselements.14.5.325, 2018.

Klunder, L., de Stigter, H., Lavaleye, M. S. S., van Bleijswijk, J. D. L., van der Veer, H. W., Reichart, G.-J., and Duineveld, G. C. A.: A Molecular Approach to Explore the Background Benthic Fauna Around a Hydrothermal Vent and Their Larvae: Implications for Future Mining of Deep-Sea SMS Deposits, Front. Mar. Sci., 7, 134, https://doi.org/10.3389/fmars.2020.00134, 2020.

Khripounoff, A., Vangriesheim, A., Crassous, P., Segonzac, M., Colaco, A., Desbruyeres, D., and Barthelemy, R.: Particle flux in the Rainbow hydrothermal vent field (Mid-Atlantic Ridge): Dynamics, mineral and biological composition, J. Mar. Res., 59, 633–656, https://doi.org/10.1357/002224001762842217, 2001.

Klindworth, A., Pruesse, E., Schweer, T., Peplies, J., Quast, C., Horn, M. and Glöckner, F. O.: Evaluation of general 16S ribosomal RNA gene PCR primers for classical and next-generation sequencing-based diversity studies, Nucleic Acids Res., 41, e1, https://doi.org/10.1093/nar/gks808, 2013.

Levin, L. A., Mengerink, K., Gjerde, K. M., Rowden, A. A., Van Dover, C. L., Clark, M. R., Ramirez-Llodra, E., Currie, B., Smith, C. R., Sato, K. N., Gallo, N., Sweetman, A. K., Lily, H., Armstrong, C. W., and Brider, J.: Defining "Serious Harm" to the Marine Environment in the Context of Deep-Seabed Mining, Mar. Policy, 74, 245–259, https://doi.org/10.1016/j.marpol.2016.09.032, 2016

López-García, P., Duperron, S., Philippot, P., Foriel, J., Susini, J., and Moreira, D.: Bacterial diversity in hydrothermal sediment and epsilonproteobacterial dominance in experimental microcolonizers at the Mid-Atlantic Ridge, Environ. Microbiol., 5, 961–976, https://doi.org/10.1046/j.1462-2920.2003.00495.x, 2003.

Ludford, E. M., Palmer, M. R., German, C. R., and Klinkhammer, G. P.: The geochemistry of Atlantic hydrothermal particles, Geophys. Res. Lett., 23, 3503–3506, https://doi.org/10.1029/96GL02078, 1996.

Mandernack, K. W. and Tebo, B. M.: Manganese Scavenging and Oxidation at Hydrothermal Vents and in Vent Plumes, Geochim. Cosmochim. Ac., 57, 3907–3923, https://doi.org/10.1016/0016-7037(93)90343-U, 1993.

Marques, A. F. A., Barriga, F., Chavagnac, V., and Fouquet, Y.: Mineralogy, geochemistry, and Nd isotope composition of the Rainbow hydrothermal field, Mid-Atlantic Ridge, Miner. Deposita, 41, 52–67, https://doi.org/10.1007/s00126-005-0040-8, 2006.

McCollom, T. M.: Geochemical constraints on primary productivity in submarine hydrothermal vent plumes, Deep-Sea Res. Pt. I, 47, 85–101, https://doi.org/10.1016/S0967-0637(99)00048-5, 2000.

Michard, G., Albarède, F., Michard, A., Minister, J. F., Charlou. J. L., and Tan, N.: Chemistry of Solution from the 13° N East Pacific Rise Hydrothermal Site, Earth Planet. Sc. Lett. 67, 297–307, https://doi.org/10.1016/0012-821X(84)90169-9, 1984.

Mino, S., Nakagawa, S., Makita, H., Toki, T., Miyazaki, J., Sievert, S. M., and Watanabe, H.: Endemicity of the cosmopolitan mesophilic chemolithoautotroph Sulfurimonas at deep-sea hydrothermal vents, ISME J., 11, 909, https://doi.org/10.1038/ismej.2016.178, 2017.

Nakagawa, S., Takai, K., Inagaki, F., Hirayama, H., Nunoura, T., Horikoshi, K., and Sako, Y.: Distribution, phylogenetic diversity and physiological characteristics of epsilon-Proteobacteria in a deep-sea hydrothermal field, Environ. Microbiol., 7, 1619–1632, https://doi.org/10.1111/j.1462-2920.2005.00856.x, 2005.

Olins, H. C., Rogers, D. R., Preston, C., Ussler, W., Pargett, D., Jensen, S., Roman, B., Birch, J. M., Scholin, C. A., Haroon, M. F., and Girguis, P. R.: Co-registered Geochemistry and Metatranscriptomics Reveal Unexpected Distributions of Microbial Activity within a Hydrothermal Vent Field, Front. Microbiol., 8, 1042, https://doi.org/10.3389/fmicb.2017.01042, 2017.

Opatkiewicz, A. D., Butterfield, D. A., and Baross, J. A.: Individual hydrothermal vents at Axial Seamount harbor distinct subseafloor microbial communities, Fems Microbiol. Ecol., 70, 413–424, https://doi.org/10.1111/j.1574-6941.2009.00747.x, 2009.

Orcutt, B. N., Sylvan, J. B., Knab, N. J., and Edwards, K. J.: Microbial ecology of the dark ocean above, at, and below the seafloor, Microbiol. Mol. Biol. Rev., 75, 361–422, https://doi.org/10.1128/MMBR.00039-10, 2011.

Phillips, B. T.: Beyond the vent: New perspectives on hydrothermal plumes and pelagic biology, Deep-Sea Res. Pt. II, 137, 480–485, https://doi.org/10.1016/j.dsr2.2016.10.005, 2017.

Ramirez-Llodra, E., Tyler, P. A., Baker, M. C., Bergstad, O. A., Clark, M. R., Escobar, E., Levin, L. A., Menot, L., Rowden, A. A., Smith, C. R., and Van Dover, C. L.: Man and the Last Great Wilderness: Human Impact on the Deep Sea, Plos One, 6, e2258, https://doi.org/10.1371/journal.pone.0022588, 2011.

Reed, D. C., Breier, J. A., Jiang, H. S., Anantharaman, K., Klausmeier, C. A., Toner, B. M., Hancock, C., Speer, K., Thurnherr, A. M., and Dick, G. J.: Predicting the response of the deep-ocean microbiome to geochemical perturbations by hydrothermal vents, Isme J., 9, 1857–1869, https://doi.org/10.1038/ismej.2015.4, 2015.

Resing, J. A., Sedwick, P. N., German, C. R., Jenkins, W. J., Moffett, J. W., Sohst, B. M., and Tagliabue, A.: Basin-Scale Transport of Hydrothermal Dissolved Metals across the South Pacific Ocean, Nature, 523, 200–203, https://doi.org/10.1038/nature14577, 2015.

Severmann, S., Johnson, C. M., Beard, B. L., German, C. R., Edmonds, H. N., Chiba, H., and Green, D. R. H.: The effect of plume processes on the Fe isotope composition of hydrothermally derived Fe in the deep ocean as inferred from the Rainbow vent site, Mid-Atlantic Ridge, 36°14′ N, Earth Planet. Sc. Lett., 225, 63–76, https://doi.org/10.1016/j.epsl.2004.06.001, 2004.

Sheik, C. S., Anantharaman, K., Breier, J. A., Sylvan, J. B., Edwards, K. J., and Dick, G. J.: Spatially resolved sampling reveals dynamic microbial communities in rising hydrothermal plumes across a back-arc basin, Isme J., 9, 1434–1445, https://doi.org/10.1038/ismej.2014.228, 2015.

Sunamura, M., Higashi, Y., Miyako, C., Ishibashi, J., and Maruyama, A.: Two bactetia phylotypes are predominant in the Suiyo Seamount hydrothermal plume, Appl. Environ. Microb., 70, 1190–1198, https://doi.org/10.1128/AEM.70.2.1190-1198.2004, 2004.

Sylvan, J. B., Pyenson, B. C., Rouxel, O., German, C. R., and Edwards, K. J.: Time-series analysis of two hydrothermal plumes at 9°50′ N East Pacific Rise reveals distinct, heterogeneous bacterial populations, Geobiology, 10, 178–192, https://doi.org/10.1111/j.1472-4669.2011.00315.x, 2012.

Thurnherr, A. M. and Richards, K. J.: Hydrography and high-temperature heat flux of the Rainbow hydrothermal site (36°14′ N, Mid-Atlantic Ridge), J. Geophys. Res.-Oceans, 106, 9411–9426, https://doi.org/10.1029/2000JC900164, 2001.

Thurnherr, A. M., Richards, K. J., German, C. R., Lane-Serff, G. F., and Speer, K. G.: Flow and mixing in the rift valley of the Mid-Atlantic Ridge, J. Phys. Oceanogr., 32, 1763–1778, https://doi.org/10.1175/1520-0485(2002)032<1763:FAMITR>2.0.CO;2, 2002.

Trocine, R. P. and Trefry, J. H.: Distribution and chemistry of suspended particles from an active hydrothermal vent site on the Mid-Atlantic Ridge at 26° N, Earth Planet. Sc. Lett. 88, 1–15, https://doi.org/10.1016/0012-821X(88)90041-6, 1988.

van Bleijswijk, J. D. L., Whalen, C., Duineveld, G. C. A., Lavaleye, M. S. S., Witte, H. J., and Mienis, F.: Microbial assemblages on a cold-water coral mound at the SE Rockall Bank (NE Atlantic): interactions with hydrography and topography, Biogeosciences, 12, 4483–4496, https://doi.org/10.5194/bg-12-4483-2015, 2015.

van Haren, H., Duineveld, G., and de Stigter, H.: Prefrontal bore mixing, Geophys. Res. Lett., 44, 9408–9415, https://doi.org/10.1002/2017GL074384, 2017.

Vare, L. L., Baker, M. C., Howe, J. A., Levin, L. A., Neira, C., Ramirez-Llodra, E. Z., Reichelt-Brushett, A., Rowden, A. A., Shimmield, T. M., Simpson, S. L., and Soto, E. H.: Scientific Considerations for the Assessment and Management of Mine Tailings Disposal in the Deep Sea, Front. Mar. Sci., 5, 17, https://doi.org/10.3389/fmars.2018.00017, 2018.

Weaver, P. P., Billett, D. S., and Van Dover, C. L.: Environmental risks of deep-sea mining, in: Handbook on Marine Environment Protection, Springer, 215–245, https://doi.org/10.1007/978-3-319-60156-4_11, 2018.

Wetzel, L. R. and Shock, E. L.: Distinguishing ultramafic- from basalt-hosted submarine hydrothermal systems by comparing calculated vent fluid compositions, J. Geophys. Res.-Sol. Ea., 105, 8319–8340, https://doi.org/10.1029/1999JB900382, 2000.

Yilmaz, P., Parfrey, L. W., Yarza, P., Gerken, J., Pruesse, E., Quast, C., Schweer, T., Peplies, J., Ludwig, W., and Glöckner, F. O.: The SILVA and "all-species living tree project (LTP)" taxonomic frameworks, Nucleic Acids Res., 42, 643–648, https://doi.org/10.1093/nar/gkt1209, 2014.

Zinger, L., Amaral-Zettler, L. A., Fuhrman, J. A., Horner-Devine, M. C., Huse, S. M., Welch, D. B. M., Martiny, J. B. H., Sogin, M., Boetius, A., and Ramette, A.: Global Patterns of Bacterial Beta-Diversity in Seafloor and Seawater Ecosystems, Plos One, 6, 63–76, https://doi.org/10.1371/journal.pone.0024570, 2011.